CONTENTS

1 INTRODUCTION

This report presents results obtained from four tests into the phenomenon of earthquake induced soil liquefaction and the resulting floatation of underground tunnels. A review of previous work in this area and the motivation for the project is also included.

1.1 MOTIVATION

Estimates suggest that worldwide there are around 500,000 earthquakes a year, of these around 100,000 will be noticed by humans. [1] As cities expand, many in areas of high seismic activity, the possibility for loss of life as a result of earthquakes is increasing. In the 21st century hundreds of thousands have already been killed as a result of earthquakes with recent notable events including:

- 2004 Indian Ocean Earthquake and Tsunami
    - 227,898 fatalities, 1.7 million people displaced [2]
- 2005 Kashmir Earthquake
    - 86,000 fatalities [3]
- 2008 Sichuan Earthquake
    - 69,195 fatalities, 5.36 million buildings collapsed [4]
- 2010 Haiti Earthquake
    - 316,000 fatalities [5]
- 2011 Tohoku Earthquake and Tsunami
    - 15,703 fatalities [6]
- 2011 Christchurch Earthquake
    - 80% of water and sewerage system severely damaged with moderate to significant liquefaction through the whole city [7]
- 2015 Nepal Earthquake
    - 8844 fatalities [8]

Figure 1 - Effects of Liquefaction Following 1964 Niigata Earthquake

The results of an earthquake can range from minor structural damage to complete failure, tsunamis, floods and fires. Another result of an earthquake can be soil liquefaction, this can lead to failure of foundations as the ground no longer provides the support required, the result of this can be seen in Figure 1. [9] Soil liquefaction can also lead to floatation of underground structures including tunnels, pipes and storage tanks. Any buoyant underground structure is at risk of floatation as result of soil liquefaction. Practical implications of floatation include disruption of underground transport systems and important sewage and fresh water infrastructure as seen in Figure 2. [10] Impact of soil liquefaction on a road surface is shown in Figure 3. [11]

Figure 2 - Floatation of Sewer Following Soil Liquefaction during the 2004 Chuetsu Earthquake

Figure 3 - Damaged Road Following 2011 Christchurch Earthquake

The motivation for this work is to learn more about soil liquefaction and the resulting tunnel floatation so that knowledge obtained may assist with development of strategies to prevent structural damage and potential loss of life as a result of this phenomenon.

1.2 AIMS

- To investigate floatation/uplift of rectangular tunnels due to earthquake induced soil liquefaction
- To establish the role of pore fluid viscosity and soil hydraulic conductivity on the tunnels uplift
- Use PIV and high speed imaging to determine soil deformation around the rectangular tunnel

1.3 LIQUEFACTION

Soil liquefaction occurs under earthquake conditions because during an earthquake the soil wants to contract. This contraction is resisted by the soils pore fluid, resulting in the generation of excess pore pressures. According to Terzaghi's Principle the result of this is a decrease in effective stress as the total stress remains constant, when pore pressure equals total stress, effective stress reaches zero and the soil is liquefied.

$$\sigma' = \sigma - u$$

σ' = Effective Stress

σ = Total Stress

u = Pore Pressure

Equation 1 - Terzaghi's Principle

Liquefaction occurs in soils with a low relative density of $I_D \approx$ 30-40% so that upon disturbance the particles are able to contract resulting in increased density. In order for pore pressure to increase the soil must also be saturated so that the pore space can be considered incompressible. Finally conditions should be considered undrained for the period of shaking meaning the soil should have a low to medium permeability of $K \approx 10^{-4}$ m/s. In order to ensure undrained conditions the loading must occur rapidly enough that pore pressures cannot dissipate, this is often the case under the cyclic conditions of an earthquake.

2 LITERATURE REVIEW

There has been much work into the phenomenon of earthquake induced soil liquefaction including projects looking specifically at the floatation of tunnels. This section aims to summarise some relevant previous works and provide some alternative sources of information on the soil liquefaction process.

2.1 LIQUEFACTION

Included here are two papers which provide further background information about earthquake induced soil liquefaction and also some of the techniques used for mitigation of liquefaction.

2.1.1 R Dobry (1989)

In this paper, 'Some Basic Aspects of Soil Liquefaction during Earthquakes' Dobry [12] describes the reasons liquefaction occurs and looks in detail at the different factors effecting the level of liquefaction occurring. This paper looks at some other observations made during soil liquefaction including sand boils where water from the pore space of liquefied soil is forced through an impervious surface layer giving the impression of boiling. Although these sand boils may be of no real engineering significance they do provide an indication of where liquefaction has occurred following an earthquake.

This paper also looks at how the volume of water expelled from a soil relates to the extent of liquefaction that has occurred and attempts to provide an explanation as to why Standard Penetration Test (SPT) correlations work for predicting liquefaction. Determining that the correlation is because penetration test results correlate very closely with the volume of water expelled by the sand during liquefaction.

2.1.2 Seed et al (2003)

'Recent Advances in Soil Liquefaction Engineering: A Unified and Consistent Framework' by Seed et al [13] covers many areas relevant to soil liquefaction. This includes detailed discussion of susceptibility and triggering potential of specific soils including correlations used to predict liquefaction, a look at the post liquefaction stability of soils and the deformation and displacement induced in soils by liquefaction.

The report also looks at techniques available for mitigation of liquefaction and highlights the need for more research in this area. Current mitigation techniques include excavation and compaction of soils where soil can either be compacted in situ or excavated and then compacted as it is put back in place. In situ ground densification makes use of techniques such as grouting to improve soil properties or vibration techniques to achieve compaction. One effect of soil liquefaction is lateral spreading of soil, this can be prevented using various structural systems. The report mentions deep foundations and reinforced shallow foundations which can be used to minimise the impact of soil liquefaction on above ground structures.

Possibly of greatest relevance to this investigation the report discusses the use of drains to prevent liquefaction. This can be considered analogous to increasing soil permeability with soil permeability being a key area of interest in this report. The effectiveness of drains depends on the permeability of the soil, although drains can prevent liquefaction by dissipating pore pressures they do not reduce settlements due to densification following an earthquake.

2.2 NUMERICAL ANALYSIS

Finite element analysis is a tool used in many areas of engineering and is a very useful technique for modelling soil liquefaction and the resulting floatation of tunnels.

2.2.1 SSC Madabhushi & SPG Madabhushi (2014)

In 2014 Madabhushi & Madabhushi used finite element analysis to model the floatation of rectangular tunnels in liquefied soil. [14] This paper looks at the excess pore pressures generated during an earthquake in a full scale tunnel. Of particular relevance to this investigation this paper also looked at the impact of soil permeability on floatation. The result of the finite element analysis showed that as permeability was increased tunnel uplift also increased until a certain point where the tunnel would settle during earthquake conditions. Figure 7 shows the plot produced using the finite element analysis.

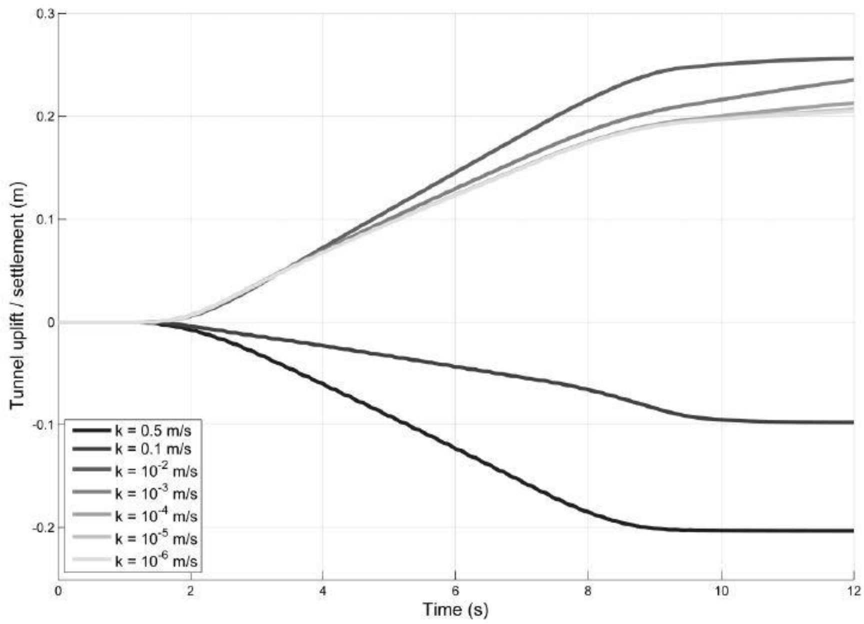

Figure 7 - Tunnel Uplift/Settlement for Varying Soil Permeabilities

This report concluded that the settlement at very high permeabilities occurred because the soils were able to dissipate significant excess pore pressures so that consolidation settlement occurred quickly drowning out the tunnel uplift.

2.3 Previous Experimental Work

Several previous investigations into floatation of tunnels as a result of earthquake induced soil liquefaction have been carried out, including two previous Cambridge MEng projects at the Schofield Centre, brief summaries of these are included here.

2.3.1 M Stringer & SPG Madabhushi (2007)

In 2007 Stringer & Madabhushi produced a paper on the modelling of liquefaction around tunnels with a circular cross section. [15] This report focussed largely on the soil mechanisms involved and the points within shaking at which soil and tunnel movement occurred. Figure 8 is a PIV plot showing soil movement between two points within one cycle of shaking.

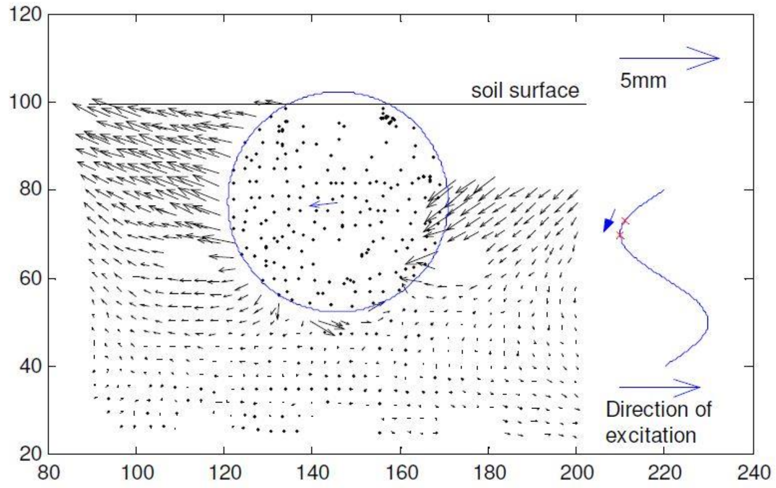

Figure 8 - Soil Displacement within a Cycle

This investigation also aims to use PIV images obtained to look at the soil displacement within a shaking cycle as well as the cumulative soil displacement for a whole test.

2.3.2 M Jenkins (2015)

Jenkins expanded on the work carried out by Room (described in section 2.3.3) in his paper completed in 2015. [16] Jenkins gathered data on the dynamic response of the tunnel in the same way that will be used in the experiments carried out here with a combination of accelerometers on the tunnel and a draw wire potentiometer to measure tunnel uplift. He also used a 'MotionBlitz' high speed camera to obtain images at a frequency of 100 Hz for use in particle image velocimetry (PIV) analysis.

The 1-g shaking table at the Schofield Centre, West Cambridge was used for all four tests carried out. For the tests carried out a shaking frequency of 4 Hz and amplitude of 3 mm was used. Much of the equipment and methods used by Jenkins will also be used in this investigation. Jenkins investigation focussed on the effect of varying tunnel depth on tunnel floatation, depth was defined as a non-dimensional number referred to as burial ratio, this is defined in Equation 2.

$$Burial\ Ratio, R_b = \frac{d}{w}$$

Equation 2 - Burial Ratio

Where d and w are defined in Figure 4.

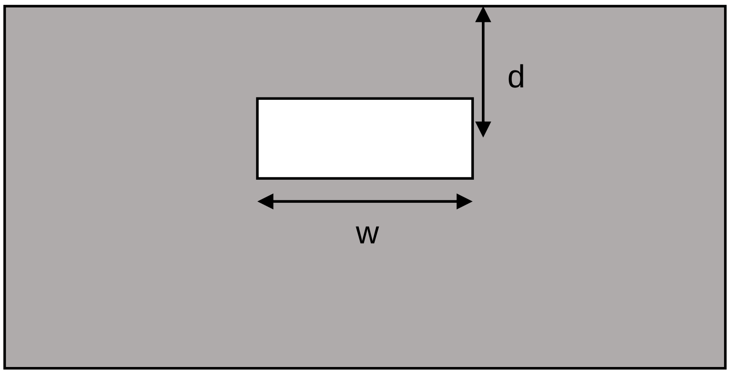

Figure 4 - Burial Ratio Dimensions

Tests were carried out at depths of R_b=0.5; 1.0; 0.25; 0.75 in this order. Jenkins results indicate that tunnel uplift during shaking increased with decreasing burial ratio. PIV analysis carried out by Jenkins also provided an indication of the soil displacements resulting from tunnel floatation. Figure 5 shows the cumulative soil displacement following his test at R_b=0.25.

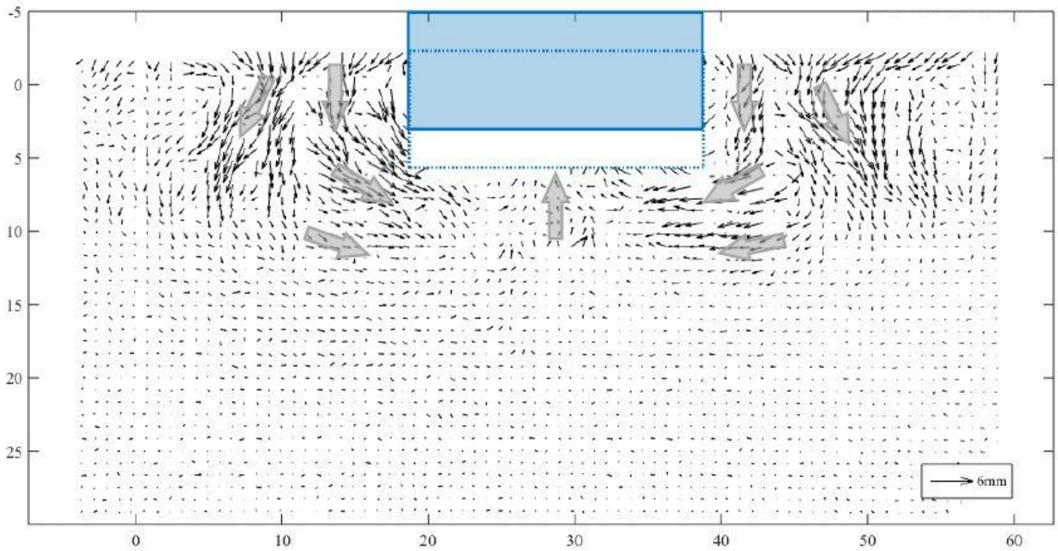

Figure 5 - Cumulative Soil Displacements for R_b=0.25

From this plot the mechanism is very clear, the PIV plot produced using images from the high speed camera is also of high quality with little information lost to wild vectors. In the tests carried out for this investigation a GoPro camera will be used and one area of interest is whether this can produce the same results as the high speed camera for dynamic tests. The GoPro is able to record higher resolution images but at a lower frequency.

In all tests carried out for this investigation a burial ratio of R_b=0.35 will be used and pore fluid viscosity will be varied for each test.

2.3.3 E Room (2014)

In 2014 Room carried out an investigation into the impact of tunnel depth on floatation in liquefied soil. [17] For Rooms investigation a sinusoidal 5 Hz input with an amplitude of 5 mm was used. The GoPro camera was used to record images at 44 FPS during all tests, these images were then used to record visual observations of the soil mechanism. Figure 6 shows the mechanism determined from the recorded images for Rooms test at R_b=0.25.

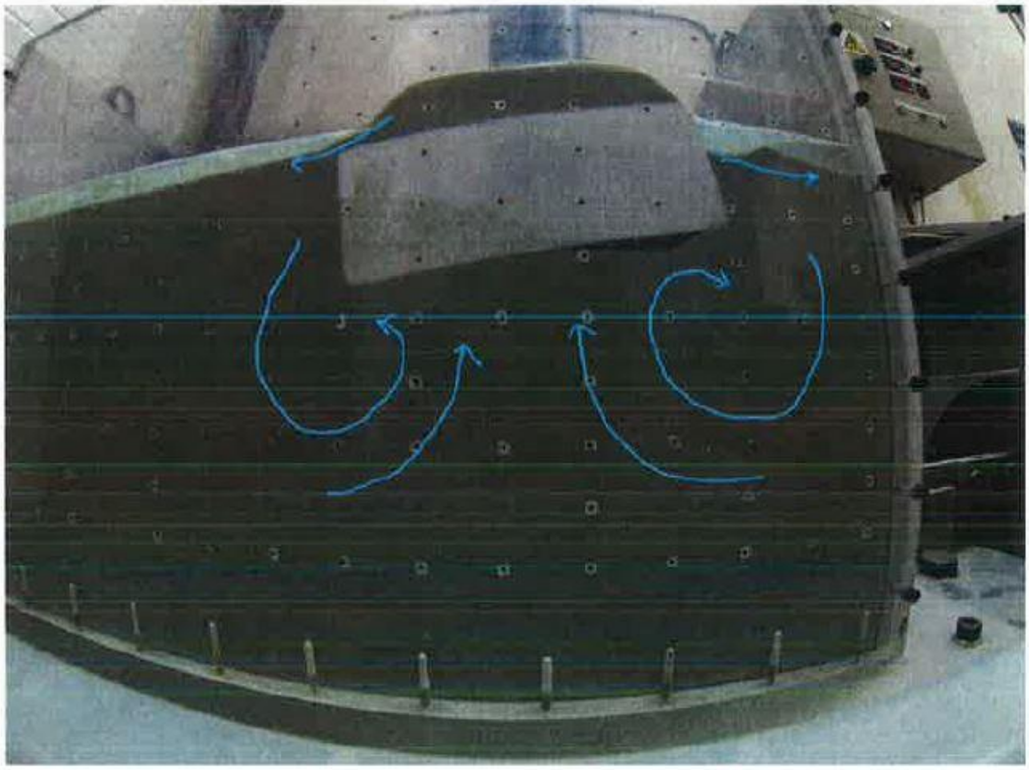

Figure 6 - Observed Soil Movement during Test at R_b=0.25

Clearly the mechanism observed here is very similar to that obtained by Jenkins using PIV. Room also used pore pressure transducers in her tests to measure excess pore pressures within the soil during shaking. These showed that significant excess pore pressures were generated, more than enough to liquefy the soil under these conditions.

For the tests carried out in this investigation pore pressure transducers were not used as none with the required level of precision were available.

3 EXPERIMENTAL SETUP

This section describes the equipment used and methods for modelling the tunnel, soil and liquefaction. Much of the equipment used is the same as or very similar to that used by Jenkins (2015) and Room (2014).

3.1 EQUIPMENT

Figure 9 shows the equipment used for all tests with a tunnel model ready for testing on the 1-g shaker table at the Schofield Centre.

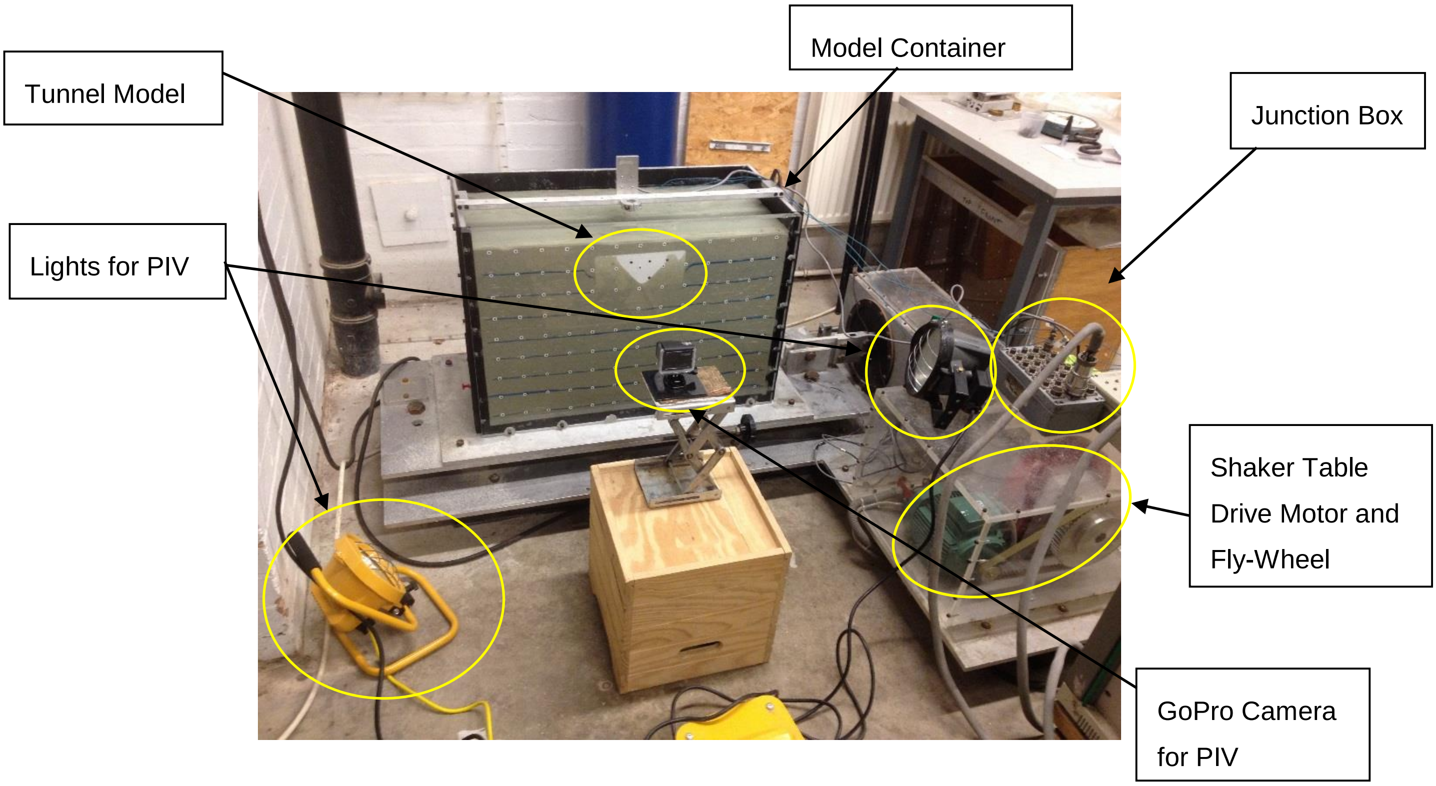

Figure 9 - Equipment Setup

3.1.1 Tunnel Model

A 300x200x80 mm aluminium box with PTFE ends. This has three piezo-accelerometers attached to it to measure vertical and horizontal acceleration, there is also a draw-wire potentiometer to measure tunnel uplift. A buoyancy calculation is included in appendix 1 and shows that the net uplift force on the tunnel is 0.007 kN at the burial ratio of 0.35.

3.1.2 Model Container

A 700 mm wide, 300 mm deep and 500 mm high waterproof container. Sand is manually poured in to this container to achieve a relative density of between 30% and 40%. Before testing the model is saturated from the base up using saturation tubes at the base of the model. On the Perspex screen there are markers for PIV calibration. A MEMS accelerometer is attached to the container to measure input acceleration and an LVDT is attached to measure input displacement.

3.1.3 Junction Box

This is connected to the computer running DASYlab software for data logging. Sensors are connected here to transfer readings to the computer.

3.1.4 Shaker Table Drive Motor and Fly-Wheel

This provides the drive for the shaker table, input frequency, amplitude and duration of shaking can be adjusted. For all tests in this investigation frequency is set to 4 Hz and amplitude to 3 mm with a 10 second shaking duration.

3.1.5 GoPro Camera

This is the camera used to record images for PIV, a 60 fps video was recorded at a resolution of 2.7K (2704x1520 pixels), this could then be broken down into stills and the images analysed using PIV.

3.1.6 Lights for PIV

PIV requires good light conditions to work effectively, these additional lights are used to ensure the PIV analysis will be successful.

3.2 Method

3.2.1 Sand Pouring

Hostun sand was used for all tests this was poured into the model container from a hopper suspended above the model. The target relative density of the sand was between 30 and 40% to ensure liquefaction would occur. This density can be controlled by varying the pour drop height and the size of the nozzle used for the pour, the correct values for these were obtained by carrying out a number of calibration pours in a container of known volume. Sand was poured alternately in the directions shown in Figure 10 to ensure consistent density was achieved.

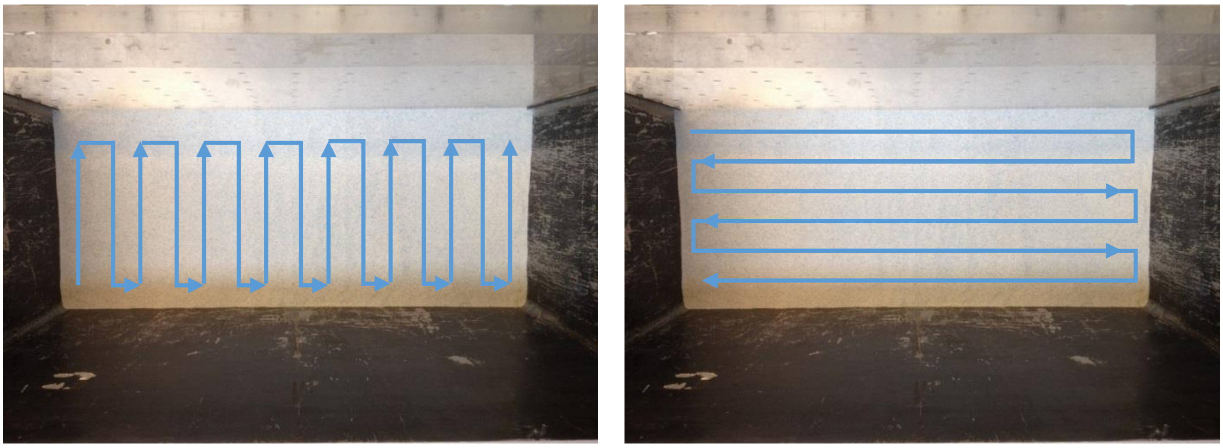

Figure 10 - Sand Pouring Direction

10% of the sand used was dyed blue in order to add extra texture to the soil for the purposes of PIV analysis. This blue sand was mixed by hand, figure 11 shows the sand before, during and after mixing.

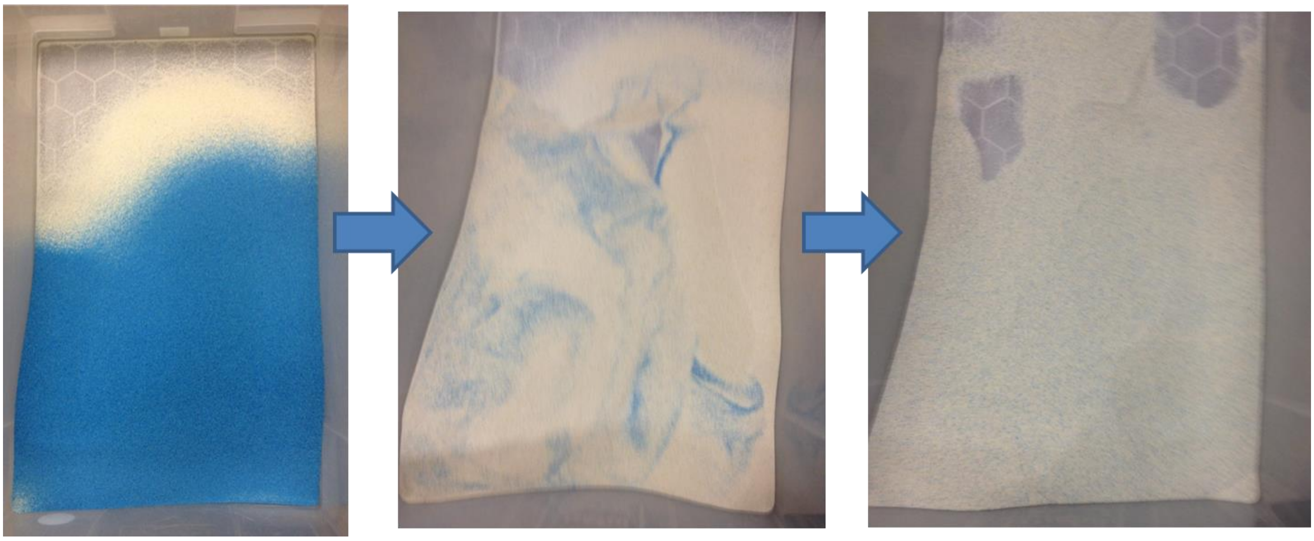

Figure 11 - Sand Mixing

During sand pouring a horizontal line of blue sand, known as a shear band, was added every 50 mm along the visible face of the container. This was to provide a clear visual representation of the soil mechanisms present. These lines are visible in the model in figure 9.

3.2.2 Saturation

The model was saturated from the base up using tubes placed at the bottom of the container and a header tank suspended above the model. The porous saturation tubes are shown in figure 12.

Figure 12 - Porous Saturation Tubes

For each test all parameters were kept constant except the viscosity of the pore fluid which was varied using different concentrations of methyl cellulose. Table 1 shows the parameters used in each test.

Table 1 – Test Conditions

Test	Burial Ratio	Target Pore Fluid Viscosity	Actual Pore Fluid Viscosity
1	0.35	1 Centistoke	1 Centistoke (Water)
2	0.35	10 Centistoke	10.7 Centistoke
3	0.35	30 Centistoke	30.2 Centistoke
4	0.35	5 Centistoke	3.8 Centistoke

Methyl Cellulose solutions were prepared using the 'hot/cold' technique as outlined in the paper by O Adamidis on preparation of viscous pore fluids for dynamic centrifuge modelling. [18] Starting points for concentration of methyl cellulose to obtain desired viscosities of fluid were also obtained from this paper, although mixtures were adjusted afterwards while measuring viscosity using a Brookfield Model DV-I + viscometer.

3.3 SHAKING

Earthquake conditions were simulated using the 1-g shaker table at the Schofield Centre in West Cambridge. A sinusoidal input with a frequency of 4 Hz and amplitude of 3 mm was used for all tests. Based on these conditions the maximum acceleration the models were exposed to can be calculated using equation 3.

$$\begin{aligned} a &= -\omega^2 d_0 \sin(\omega t) \\ &= 64\pi^2 \times \frac{3}{1000} \times 1 \\ &= 1.89\ m/s^2 \end{aligned}$$

Equation 3 - Maximum Acceleration

4 DATA ACQUISITION

For this project data acquisition can be divided into two sections, instrumentation and PIV. With instrumentation being concerned with the physical movement of the tunnel and PIV focusing on the soil mechanisms surrounding the tunnel.

4.1 INSTRUMENTATION

Figure 13 shows a diagrammatic layout of the instrumentation used for the test in the investigation.

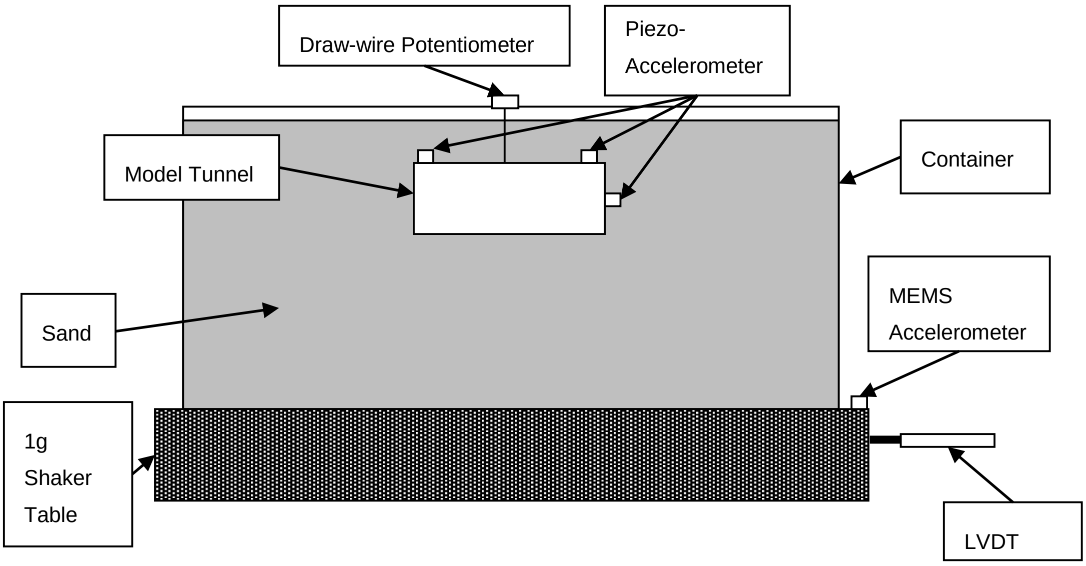

Figure 13 - Diagram of Instrumentation

4.1.1 Piezoelectric Accelerometers

Three piezoelectric accelerometers were used for the tests in the investigation, these were all attached to the tunnel. Two measure vertical acceleration of the tunnel and one measured horizontal acceleration.

4.1.2 Draw-wire Potentiometer

One draw-wire potentiometer was used for all tests, this was attached to the tunnel model and used to measure vertical displacement of the tunnel.

4.1.3 Microelectromechanical System (MEMS) Accelerometer

One MEMS accelerometer was used in all tests, this was attached to the 1-g shaker table and used to measure the input acceleration.

4.1.4 Linear Voltage Displacement Transducer (LVDT)

One LVDT was used for these tests, this measured the input displacement of the shaker table.

4.1.5 Soil Surface Profile Measurement

Soil surface profile was measured manually before and after all tests in order to obtain data about the change in soil surface profile following tunnel floatation.

4.1.6 Instrument Calibration

All instruments listed here provide a raw voltage output and this must be adjusted using calibration factors in order to provide meaningful data. Calibration was carried out on all instruments by providing either a known displacement or acceleration and then measuring voltage output while varying the input. Signals produced by these instruments are also vulnerable to noise making obtaining real data difficult, MatLab was used to process all data and filtering to remove noise was also carried out here.

4.2 PARTICLE IMAGE VELOCIMETRY (PIV)

GeoPIV software is a MatLab module which measures displacement fields from digital images. PIV is a technique originally developed for use in experimental fluid mechanics. GeoPIV was developed for use in geotechnical applications by White, Take and Bolton. PIV works by dividing images into a number of patches, each of these patches has a specific texture of colour and brightness. Each patch can be tracked in u-v (pixel) space with respect to a reference image, if this process is repeated for all images recorded during a test a profile of soil movement during the test can be established. Figure 14 [19] summarises this process.

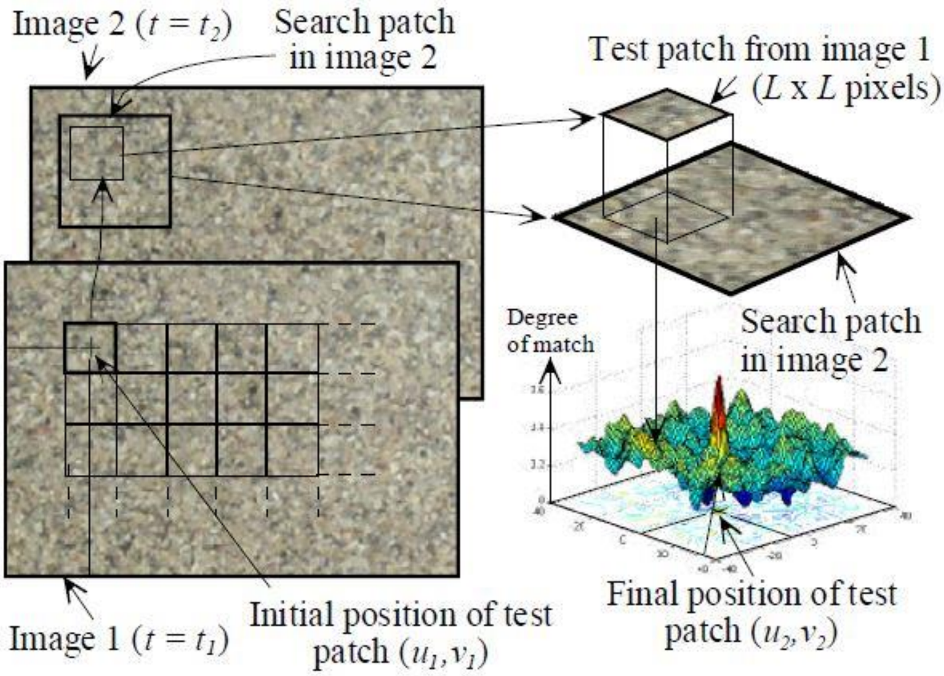

Figure 14 - Principles of PIV Analysis

Results of image processing can be displayed in a quiver plot and offer an order-of-magnitude increase in accuracy and precision compared with previous image-based methods of displacement measurement. [20]

Once patch movement is established in u-v space it can be converted to x-y (millimetre) space using calibration images which determine the positions of control markers using a Mylar card. Figure 15 shows a calibration image for Test 3.

Figure 15 - Calibration Image from Test 3

Control markers which can be tracked during the test are placed on the Perspex, for the calibration image a Mylar card is placed behind the control markers. This card is covered in dots of known spacing which can be used to determine the positions of the control markers in x-y space. As the control marker positions are tracked throughout the test this allows the position and movement of the patches in x-y space to be established.

One objective of this investigation was to determine whether the GoPro camera could record images at a high enough frequency for PIV processing of images from dynamic tests. If images are of too poor quality or there is too much movement of soil between images recorded during a test the software will struggle to track patches. The result of this will be the production of wild vectors which indicate soil movement that is unfeasible relative to other movement recorded. Due to the nature of the process some wild vectors are always expected however quality of images and parameters for which the program should run within can influence the effectiveness of the soil tracking.

5 Tunnel Response

This section looks at the movement of the tunnel model during and after each test.

5.1 Test 1 - Viscosity 1 Centistoke

Figure 16 shows the tunnel in test 1 before and after shaking, clearly the tunnel has floated and the basic soil mechanism is visible from the movement of the blue lines in the model.

Figure 16 - Test 1 Before and After Shaking

Figure 17 shows the vertical displacement of the tunnel over the course of the shaking.

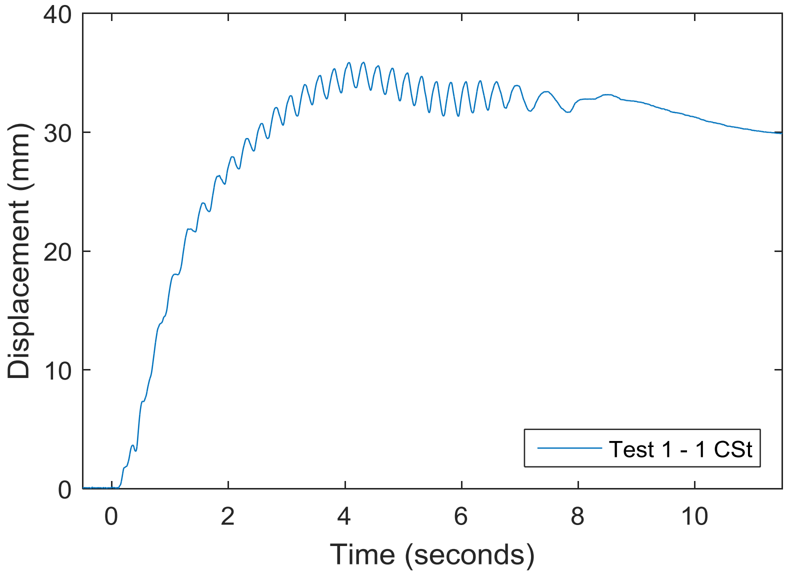

Figure 17 - Vertical Displacement vs Time for Test 1

This plot indicates that floatation began at almost the same instant as shaking. The oscillations visible on the plot are likely to be partially a result of horizontal movement of the tunnel extending and contracting the draw-wire. Although this may also be due to actual downwards movement of the tunnel during shaking. From this plot it is also clear that following peak uplift the tunnel will settle slightly as it reaches equilibrium. The results show that the peak uplift for this test was 35.9 mm and the final uplift was 29.9 mm. Figure 18 shows the vertical acceleration of the tunnel model during the test.

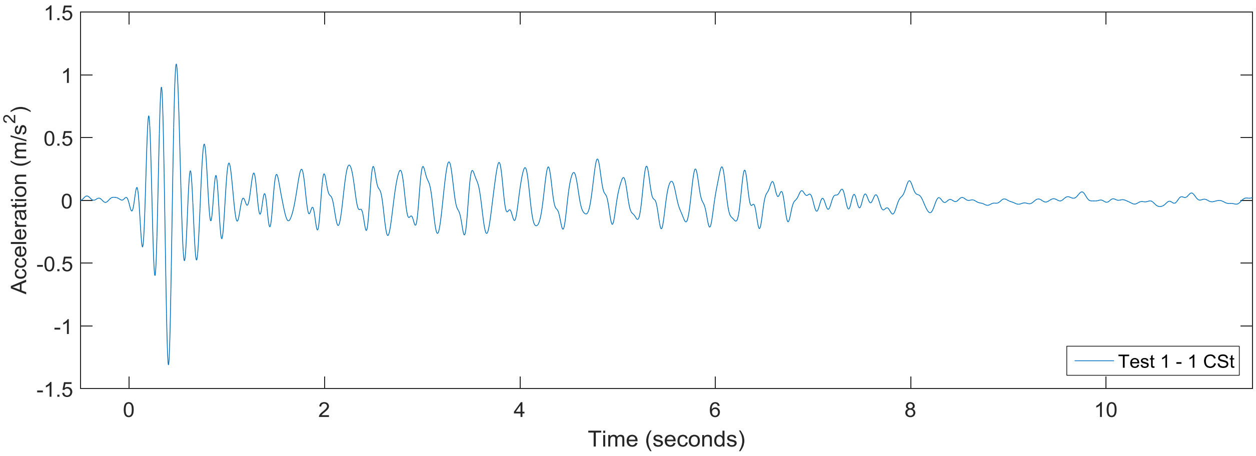

Figure 18 - Vertical Acceleration vs Time for Test 1

This clearly shows that peak accelerations occurred at the start of the test. The plot also shows that acceleration oscillates between 0.5 and -0.5 m/s^2 in the same region where oscillations occurred in figure 17, this suggests that the tunnel was moving downwards for short periods during shaking. Figure 19 shows the horizontal acceleration of the tunnel and the input acceleration of the shaker table.

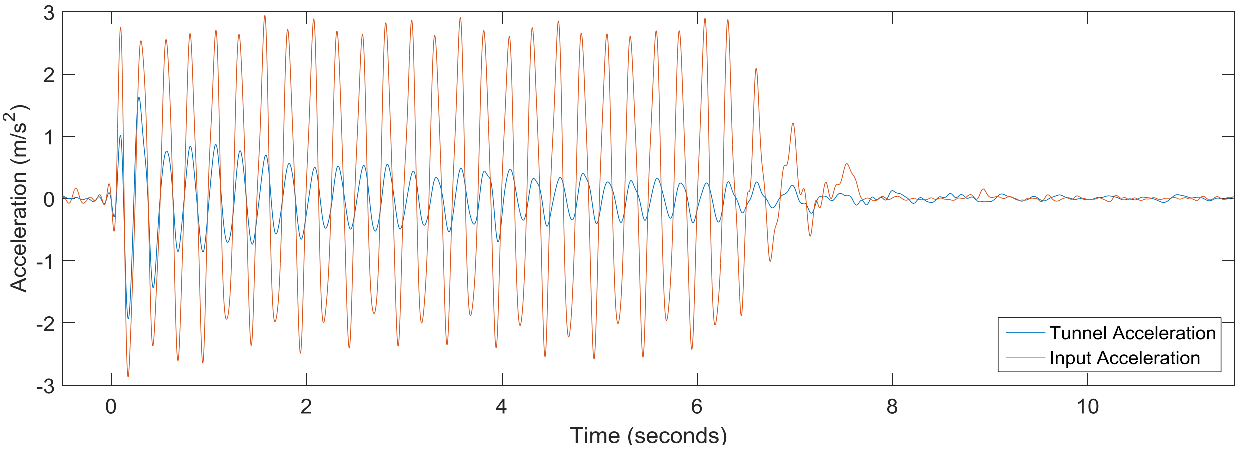

Figure 19 - Horizontal Acceleration vs Time for Test 1

From this data it is clear that tunnel acceleration was maximum near the start of the test and then decreased while the input remained constant, this is likely to be because as the soil fully liquefied the horizontal force transferred to the tunnel was lower. It is also interesting to note that in this test the acceleration of the tunnel remained in phase with the input acceleration.

Figure 19 also shows that the input acceleration was greater than the 1.89 m/s^2 expected based on the conditions. Figure 20 shows the LVDT plot of input displacement, this is higher than the expected 3 mm at 3.76 mm, while the frequency is correct at 4 Hz. Using this higher amplitude in equation 3 gives an acceleration of 2.38 m/s^2 closer to that indicated by the MEMS accelerometer on the shaker table.

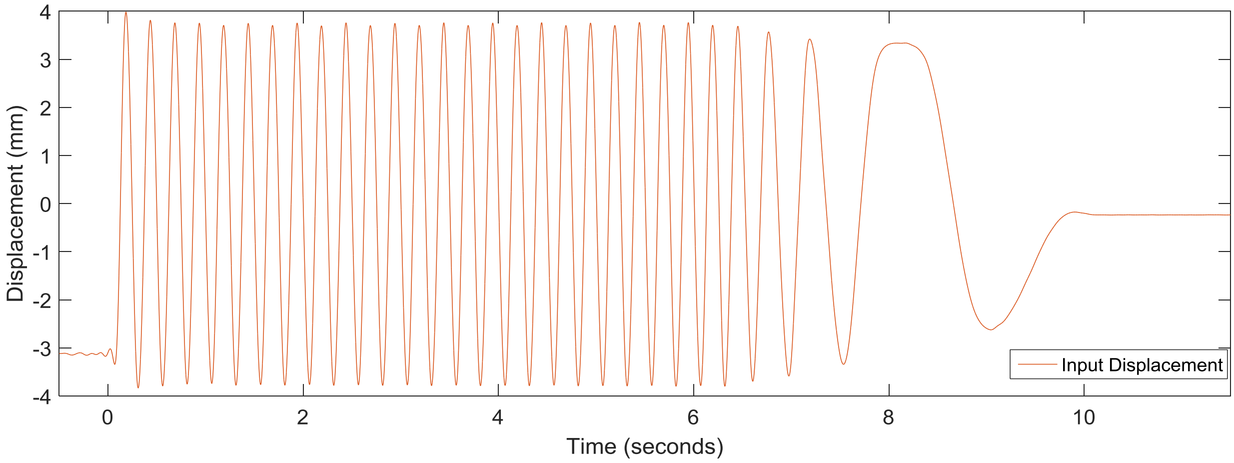

Figure 20 - Horizontal Input Displacement for Test 1

Looking at figure 16 you can see that before this test began sand fell between the tunnel face and the Perspex, this obscured the view of the tunnel. For all future tests the visible tunnel face was covered with a layer of clear grease to prevent this from happening. The tunnel with grease in place is shown in figure 21.

Figure 21 - Tunnel with face Greased

5.2 Test 2 – Viscosity 10.7 Centistoke

Figure 22 shows test 2 before and after shaking. The grease has clearly been effective in preventing the sand obscuring the tunnel face. In contrast to test 1 there is much less visible uplift of the blue shear bands, this may be a result of the higher viscosity reducing the upwards movement of the fluid during the test.

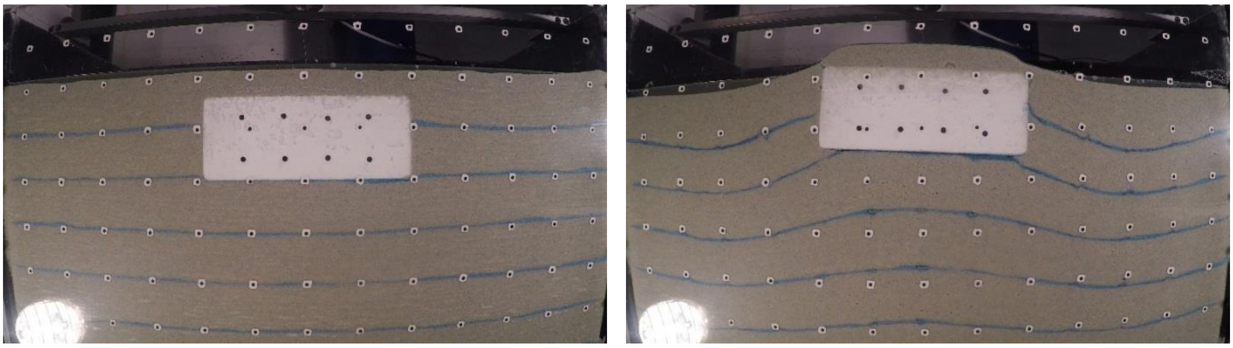

Figure 22 - Test 2 Before and After Shaking

Figure 23 shows the vertical displacement of the tunnel during the test, the result from test 1 is also shown for comparison.

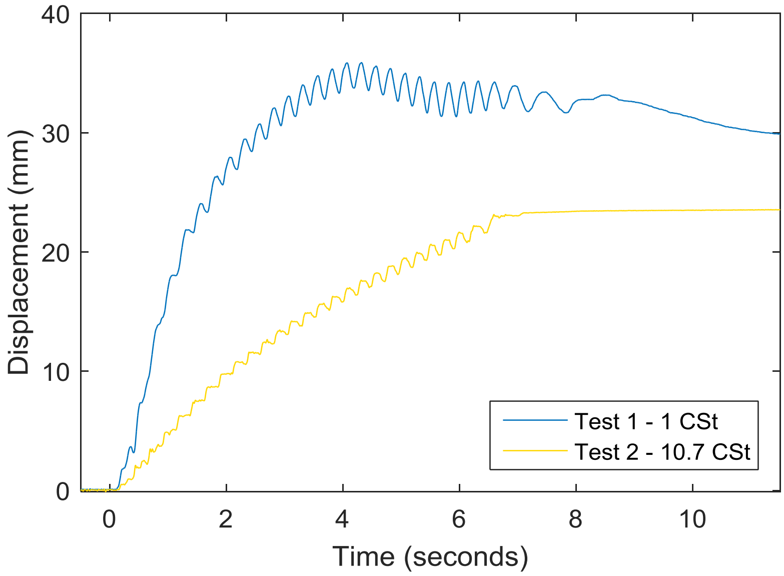

Figure 23 - Vertical Displacement vs Time for Test 2

It is clear from this data that the higher viscosity fluid reduced the tunnel uplift and also the rate of uplift. The maximum and final uplift was 23.5 mm. The additional suction on the base of the tunnel due to the higher viscosity fluid is likely to account for the reduced uplift and rate of uplift. Figure 24 shows the vertical acceleration of the tunnel for test 2 with the results from test 1 also shown for comparison.

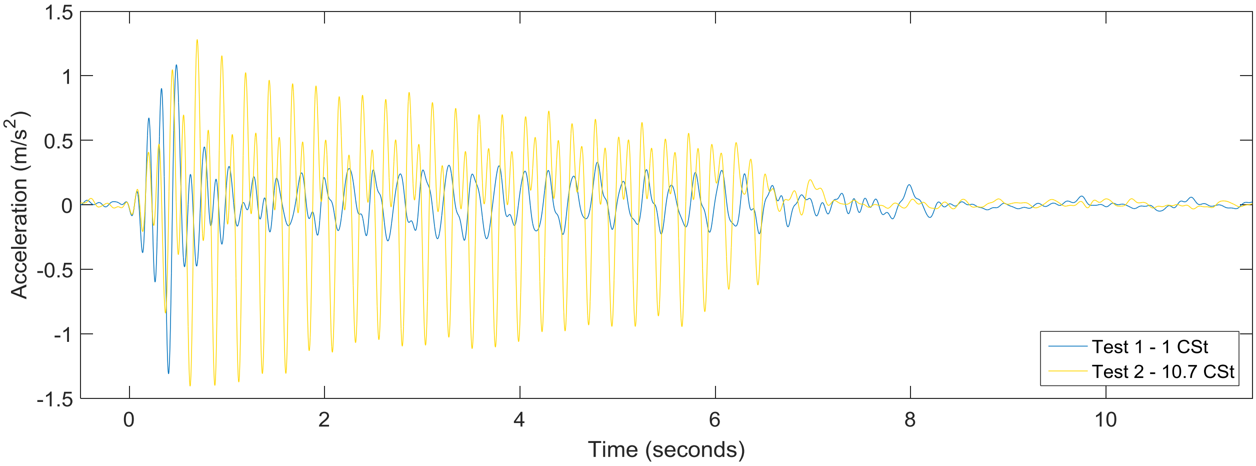

Figure 24 - Vertical Acceleration vs Time for Test 2

In contrast to test 1 the acceleration remained relatively constant with only a slight reduction as the test went on. This makes sense when looking at the vertical displacement plot as the tunnel rose relatively steadily before reaching peak uplift. The increased duration of higher accelerations is because the tunnel in test 1 reached maximum uplift relatively quickly whereas in test 2 uplift continued throughout the test. Figure 25 shows the output from the piezo accelerometer measuring horizontal acceleration, clearly there was a problem with this sensor which prevented any data being gathered.

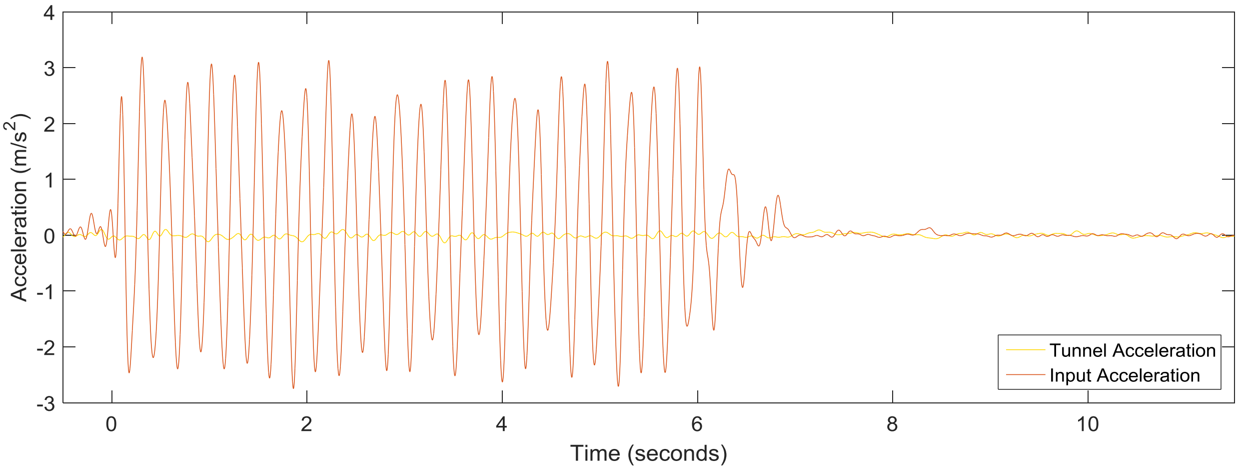

Figure 25 - Horizontal Acceleration vs Time for Test 2

Following this test the piezo accelerometer was tested and appeared to be working normally, at this stage the problem with this data was assumed to be the result of a poor connection between the sensor and the data logger.

5.3 Test 3 – Viscosity 30.2 Centistoke

Figure 26 shows the tunnel model in test 3 before and after shaking. Here it is clear that there has been even less soil movement than in test 2, as indicated by the blue shear bands.

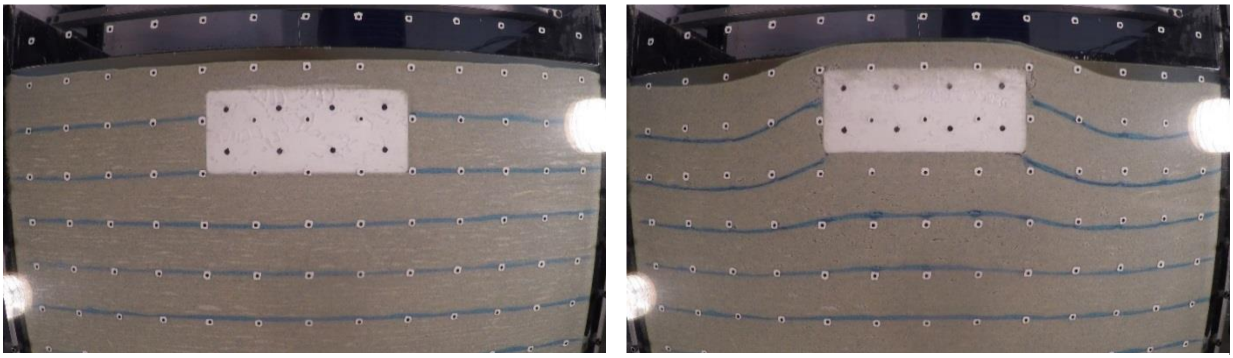

Figure 26 - Test 3 Before and After Shaking

Figure 27 shows the vertical displacement of the tunnel during test 3, the data from the two previous tests is also shown for comparison.

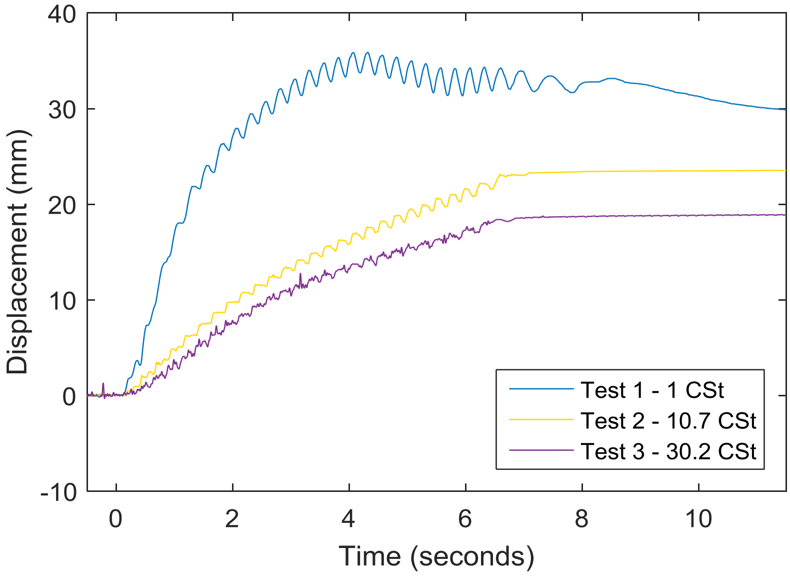

Figure 27 - Vertical Displacement vs Time for Test 3

Figure 27 clearly shows that the tunnel in test 3 floated less than that in both previous tests carried out at lower viscosities. The maximum uplift achieved in test 3 was 18.9 mm and in the same manner as test 2 this was also the final uplift. The relationship between viscosity and uplift is not linear as a threefold increase in viscosity only decreased uplift by a relatively small amount.

Figure 28 shows the vertical acceleration experienced by the tunnel with vertical acceleration from both previous tests shown for comparison.

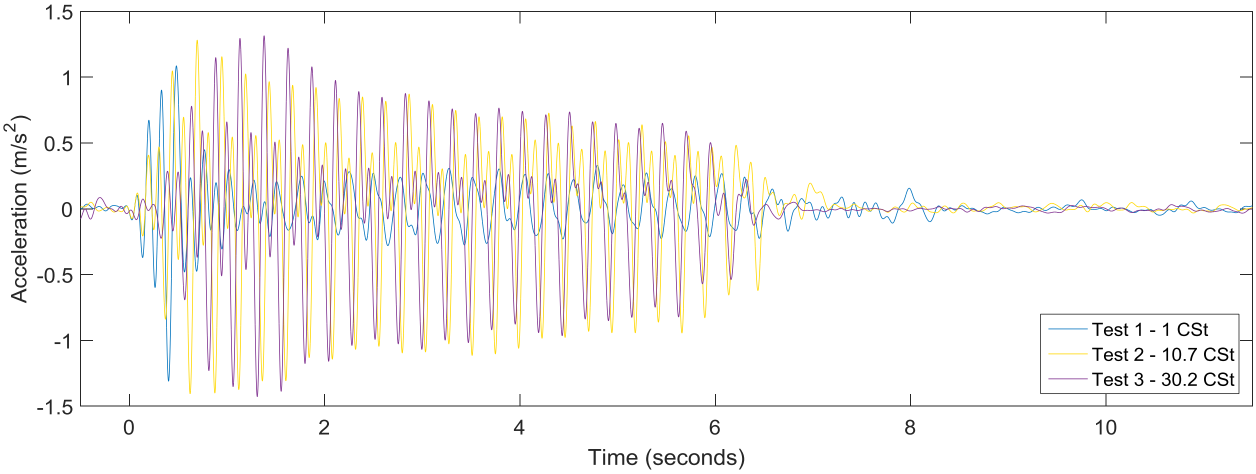

Figure 28 - Vertical Acceleration vs Time for Test 3

The vertical tunnel acceleration for test 3 is very similar to that of test 2 with a peak near the beginning of the test and then steadily reducing acceleration until the end of the test. One slight difference between the two data sets is that the peak acceleration in test 3 occurred slightly further into the test than in test 2, this may have been because at increased fluid viscosity there was a greater suction force acting on the base of the tunnel which led to increased time for maximum acceleration to occur.

Unfortunately the piezo accelerometer for measuring horizontal acceleration of the tunnel again produced no data for this test, following this test it was tested again and shown to be operating normally. For test 4 it was moved to a different channel of the junction box and tested prior to use, during the test again no data was produced so there is no plot of horizontal acceleration for test 4.

5.4 Test 4 – Viscosity 3.8 Centistoke

Figure 29 shows the model in test 4 before and after shaking. The result here appears at first glance to be most similar to test 3, indicating that the relationship between pore fluid viscosity and tunnel uplift may not be as simple as suggested by the first three tests. As with test 3 at 30.2 CSt there has been very little movement of the shear bands beneath the tunnel.

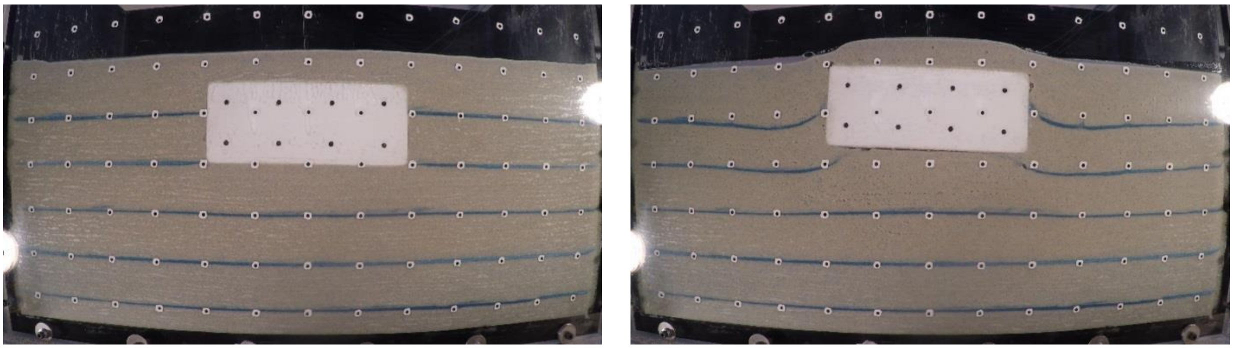

Figure 29 - Test 4 Before and After Shaking

Figure 30 shows the vertical displacement of the tunnel throughout the test along with the results of previous tests for comparison.

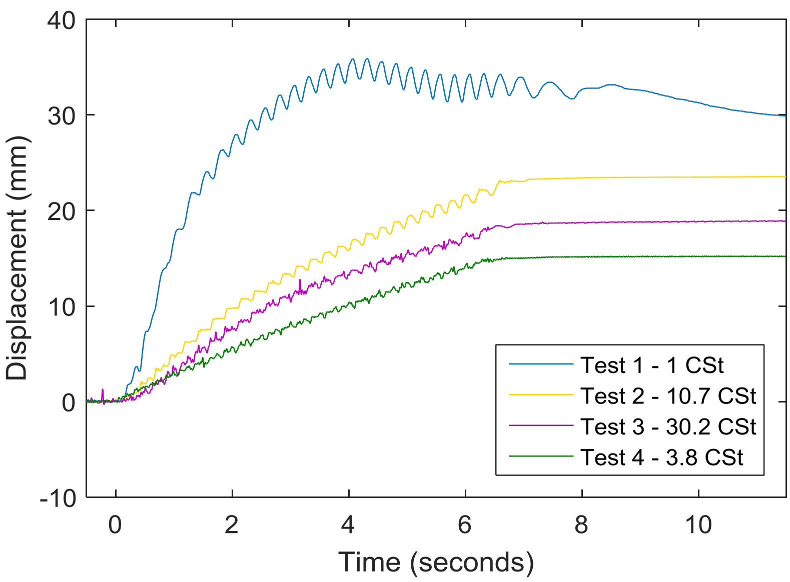

Figure 30 - Vertical Displacement vs Time for Test 4

The result here clearly shows that the tunnel in test 4 suffered the lowest uplift at 15.2 mm. Looking closely at the data early on in the test the tunnel in test 4 moved upwards more quickly than in tests 2 and 3. A possible explanation for this could be that in test 4 the suction force due to increased pore fluid viscosity was lower than in tests 2 and 3 leading to greater uplift early in the test, however at the lower viscosity pore pressures were able to disperse more easily leading to lower overall uplift. An alternative explanation is that there was some experimental error, an example could be differences in the sand density. If the sand was denser than in previous tests then a lower uplift would be expected, it is quite possible this was the case as the sand pouring is in no way an exact science and achieving consistent density is very difficult. At the Schofield Centre there is an automatic sand pourer which provides much more consistent sand density than manual pouring, however for the level of this investigation manual pouring was considered sufficient. Ideally this test would be repeated to check for errors, if the same result was found again it would be interesting to carry out a number of tests while increasing viscosity at 1 CSt increments to establish a pattern of tunnel uplift vs viscosity in this range.

Figure 31 shows the vertical acceleration of the tunnel in test 4, along with previous results for comparison. (Test 1 results have been excluded to make the data easier to read)

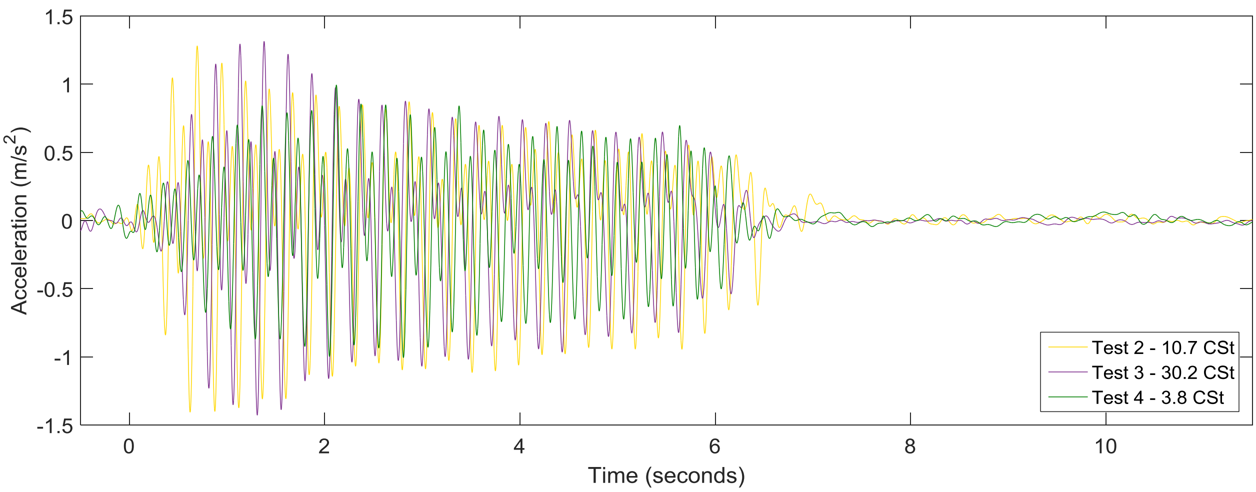

Figure 31 - Vertical Acceleration vs Time for Test 4

The results shown in figure 31 indicate that at the very beginning of the test the acceleration of the tunnel in test 4 was greater than that experienced by the tunnel in both tests 2 and 3. This lends some credibility to the explanation suggested above, although the difference early on is very small, enough so that it could even be due to noise. The peak acceleration experienced by the tunnel in test 4 was lower than in previous tests, the acceleration also remained relatively constant throughout shaking, in contrast to previous tests.

5.5 COMPARISON OF RESULTS

Clearly the key output observed in these tests is the tunnel uplift, figure 32 shows the tunnel uplift vs viscosity for the 4 tests.

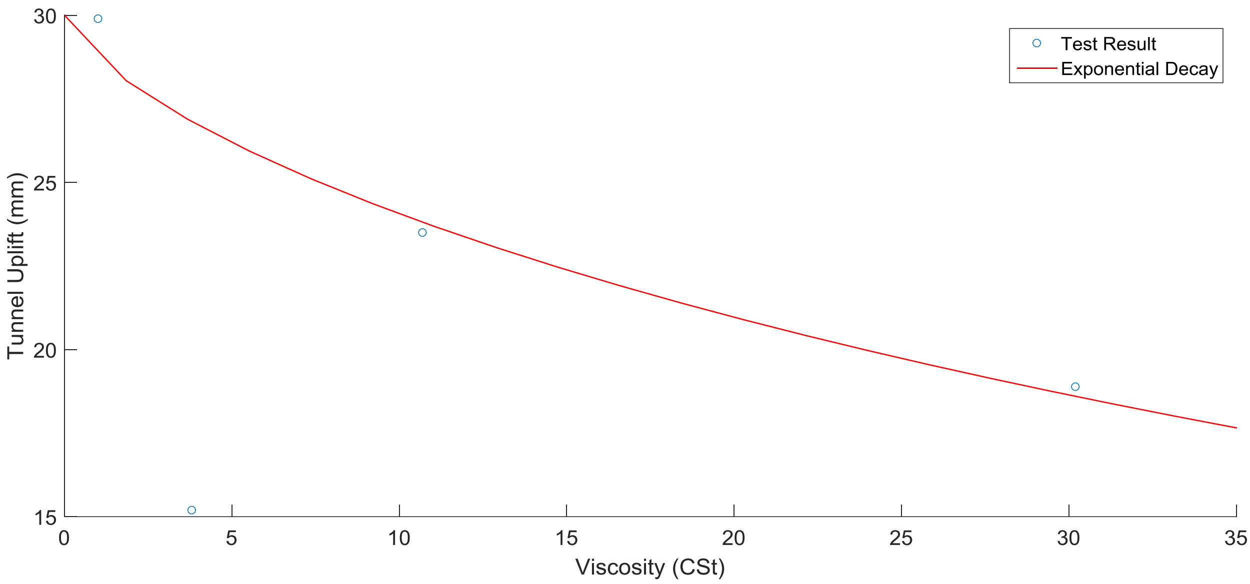

Figure 32 - Tunnel Uplift vs Viscosity for Tests 1-4

Excluding the result of test 4 the tunnel uplift decays roughly exponentially as viscosity is increased. The equation for this exponential decay is shown in equation 4.

$$y = 30e^{(-0.044x^{0.7})}$$

$$y = Tunnel\ Uplift$$

$$x = Pore\ Fluid\ Viscosity$$

Equation 4 - Equation for Exponential Decay of Tunnel Uplift

Based on this tunnel uplift should be negligible with pore fluid viscosity above a certain value. This increasing viscosity is equivalent to decreasing permeability so the results suggest that in low permeability soils no floatation should occur. This is the case in reality as soil liquefaction does not occur in clayey or silty sold where permeability is very low.

6 SOIL DEFORMATION

This section looks at the displacement experienced by the soil using both the results obtained from the PIV processing and the manual measurements made of the soil surface profile.

6.1 TEST 1 – VISCOSITY 1 CENTISTOKE

Figure 33 shows the soil surface profile plot for test 1 before and after shaking.

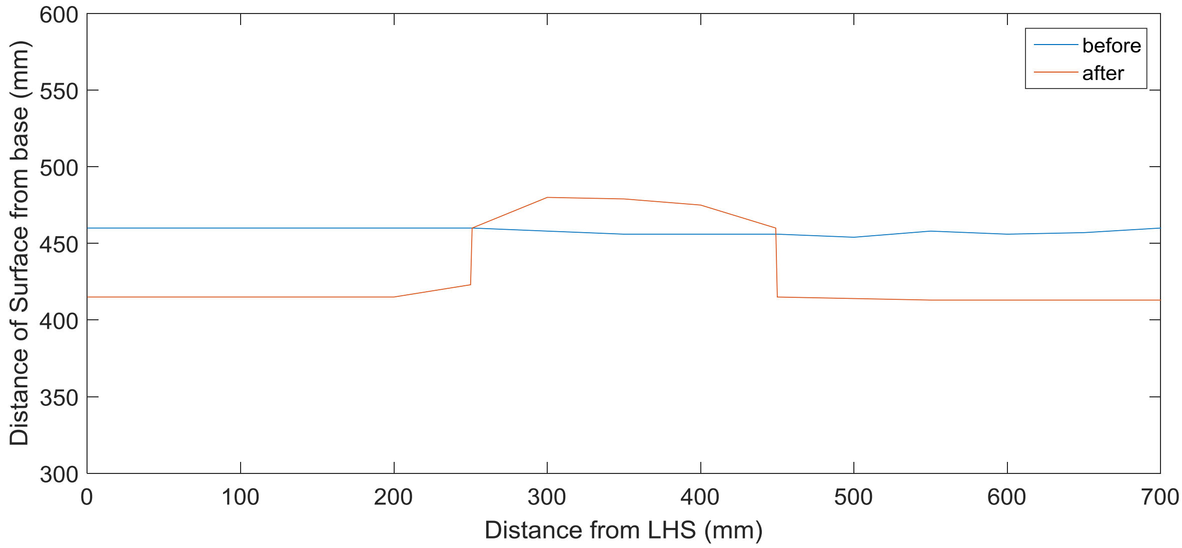

Figure 33 - Soil Surface Profile for Test 1

Here it is clear that the soil surrounding the tunnel has settled, some of this soil has moved beneath the tunnel and some settlement has occurred due to densification of the soil. The maximum settlement that has occurred is 47 mm.

For test 1 it was not possible to produce a cumulative PIV plot of the soil displacement as this resulted in almost complete loss of data due to wild vectors. The camera position and settings were adjusted for the following tests allowing a plot for this to be produced. As test 1 used water as the pore fluid the PIV plot from Jenkins (2015) test 3 at burial ratio of 0.25 gives a good idea of what should have occurred in test 1 for the purposes of comparison with the other tests. This is included as figure 34. [16]

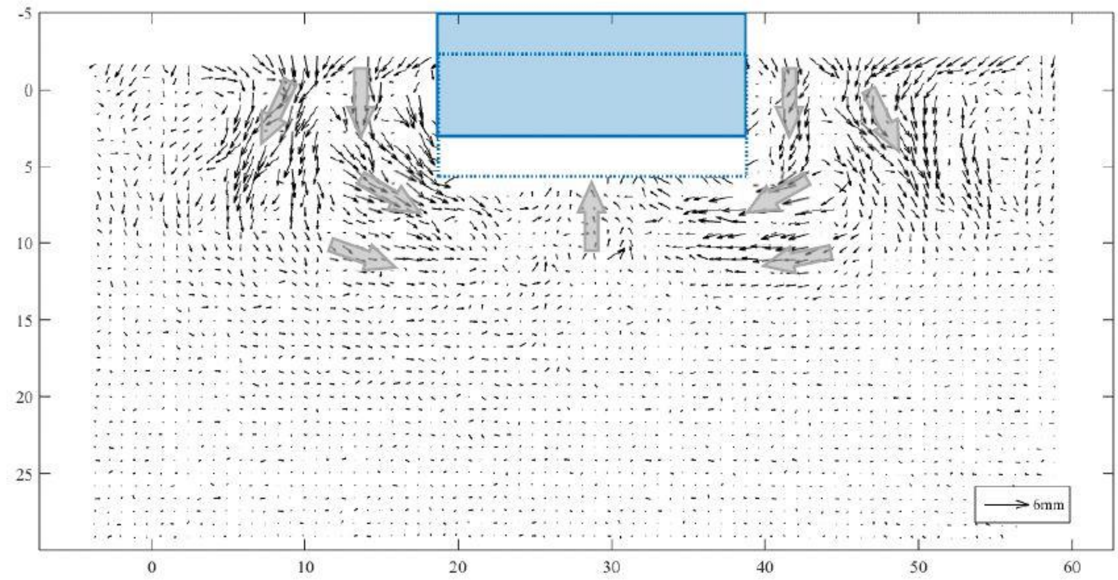

Figure 34 – Cumulative Soil Displacement for Viscosity 1 CSt at R_b=0.25

Figure 35 shows the soil displacement for the first quarter cycle of shaking in test 1.

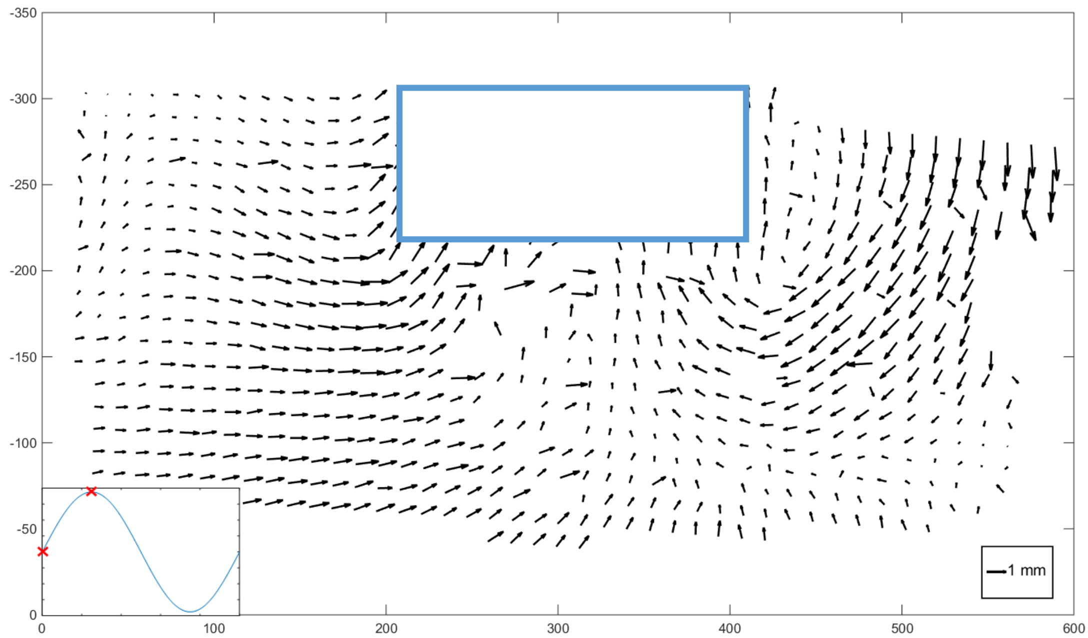

Figure 35 - First Quarter of Cycle for Test 1

At this stage the shaking table has moved fully to the left, this plot shows that the soil in the left of the model has moved to the right relative to the whole model and soil on the right has moved downwards and to the left. Some uplift has already occurred at this stage with soil immediately beside the tunnel also being drawn upwards. All movements at this stage are very small, mostly less than 1 mm. Figure 36 shows the next quarter cycle for test 1.

The PIV plot shows that at this point all the soil was moving to the left relative to the model which was moving to the right, with the exception of an undisturbed zone in the bottom left corner of the model. The movement magnitudes are more than twice as large as those experienced in the first quarter of the cycle. There also appears to be less uplift occurring here, soil on the left of the model is moving upwards as it meets the side of the container and has no where else to go.

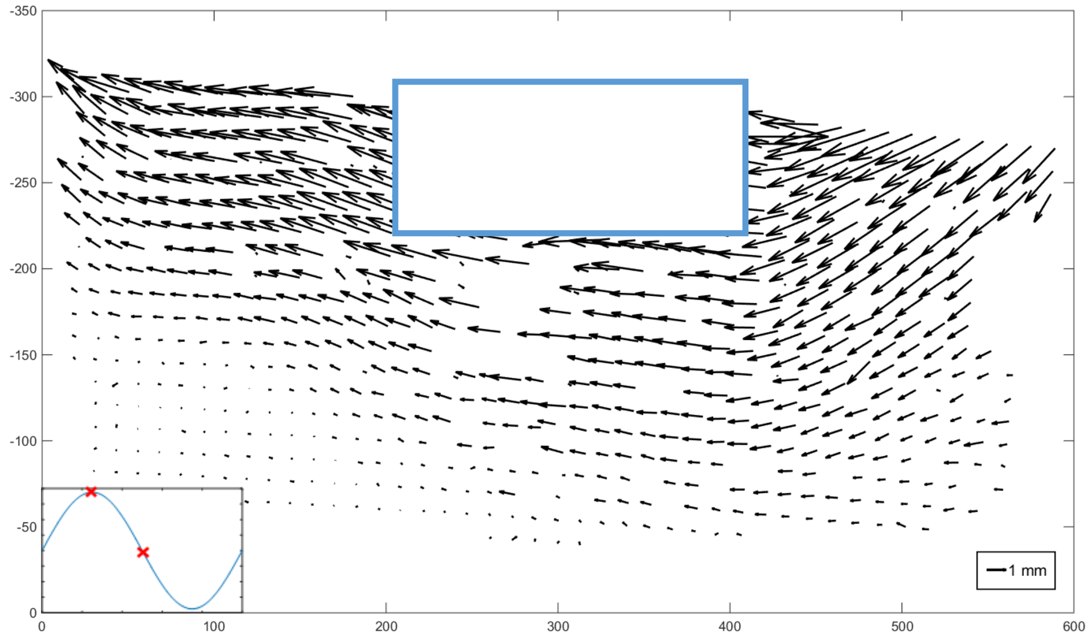

Figure 36 - Second Quarter of Cycle for Test 1

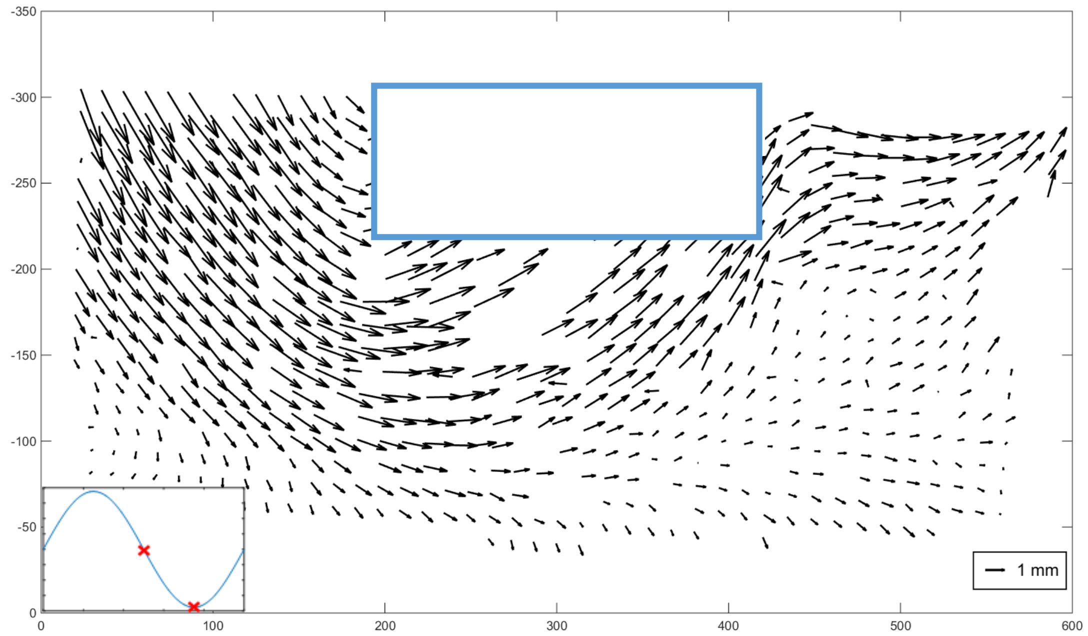

Figure 37 - Third Quarter of Cycle for Test 1

Figure 37 shows the soil displacement for the third quarter cycle. This is almost a mirror image of the movement in the second quarter, the key difference is that many of the vectors have a larger downwards component due to settlement of the soil.

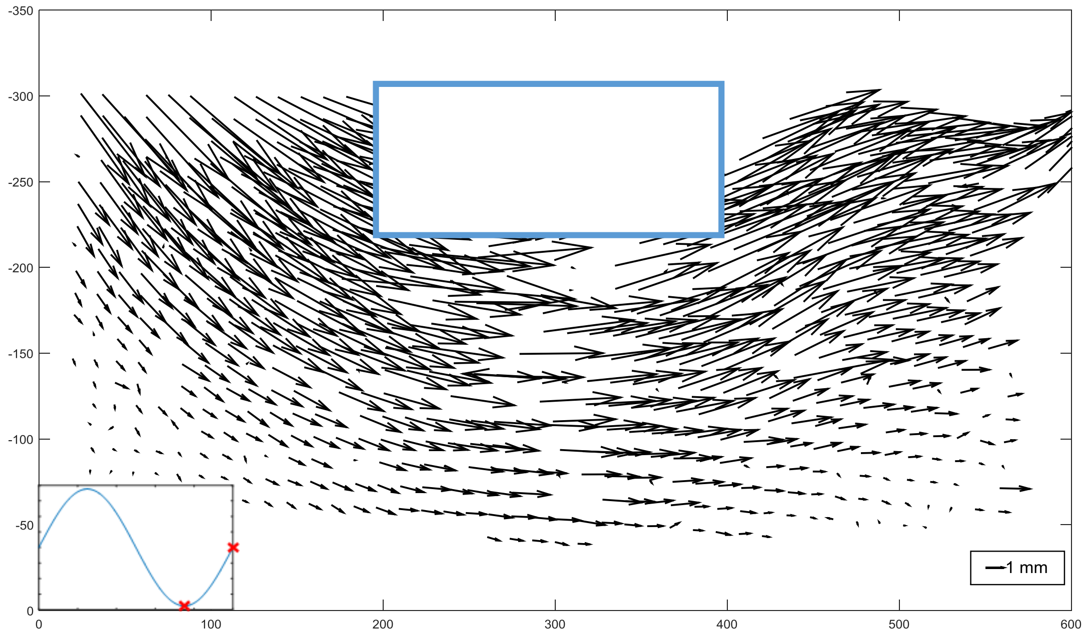

Figure 38 - Fourth Quarter of Cycle for Test 1

Figure 38 shows the fourth quarter of the shaking cycle for test 1. Here the magnitude of the vectors has increased significantly from the start of the cycle indicating that the soil has now liquefied. There is significant downwards movement of the soil except at the extreme right of the model where the soil moves upwards as it reaches the side of the model.

6.2 Test 2 – Viscosity 10.1 Centistoke

Figure 39 shows the soil surface profile before and after test 2, the maximum soil settlement that occurred was 19 mm.

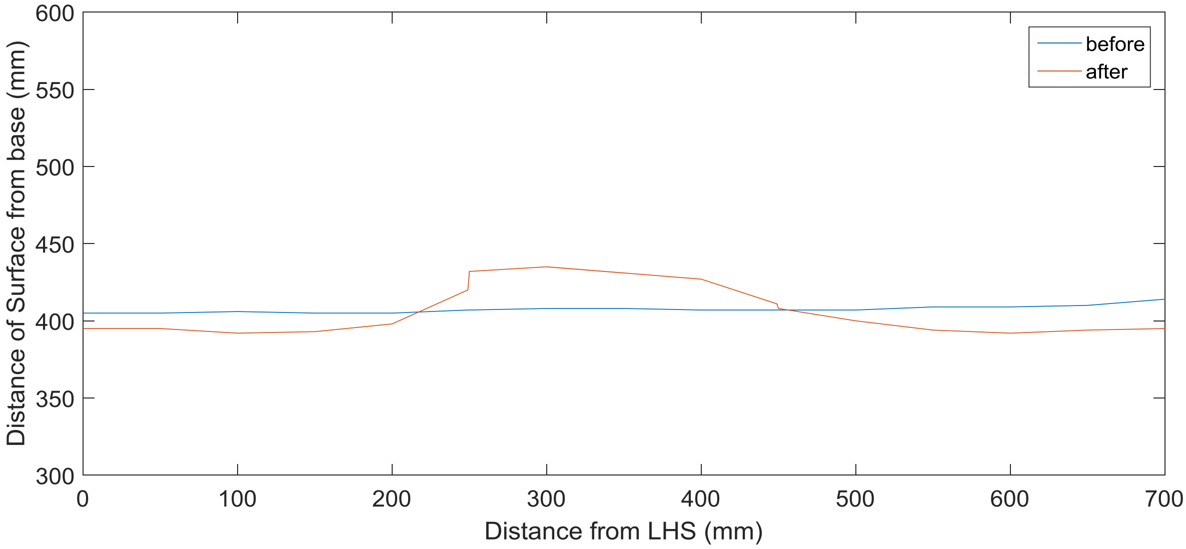

Figure 39 - Soil Surface Profile for Test 2

Figure 40 shows the cumulative soil displacement for test 2, the overall mechanism is similar to that observed in Jenkins (2015) test, except that in this plot there is noticeable cyclic movement of the soil in the regions either side of the tunnel. The quality of the PIV data produced was clearly higher in Jenkins test using the high speed camera than in the tests conducted here using the GoPro. The plot of cumulative soil displacement has lost more data to wild vectors in these tests.

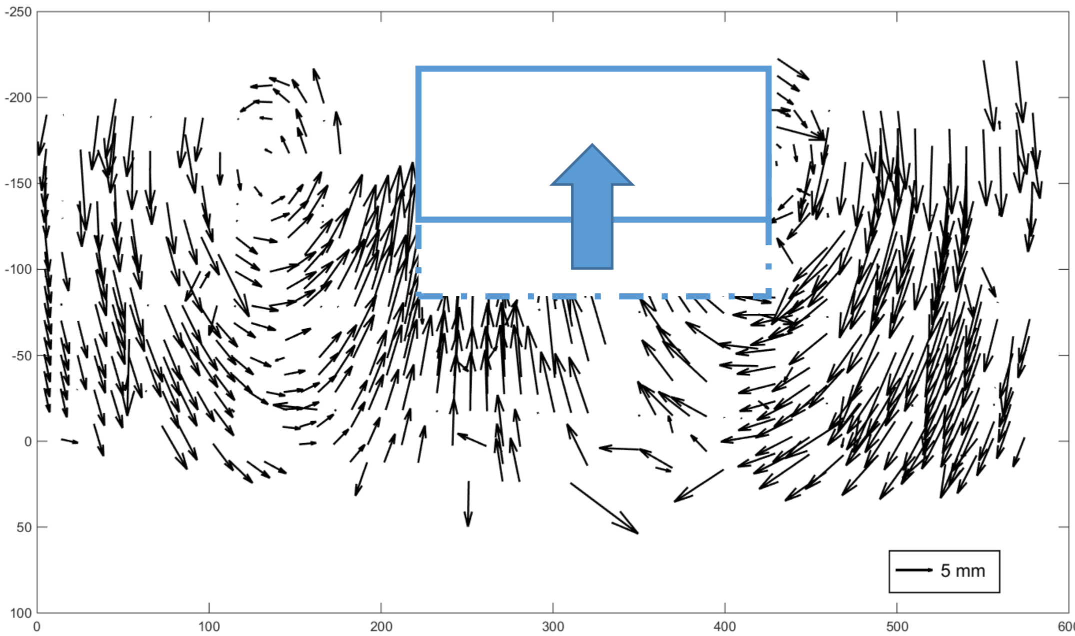

Figure 40 - Cumulative Soil Displacement for Test 2

Figure 41 shows the soil displacement for the first quarter cycle of test 2. This is quite clearly different to test 1 as all soil is moving to the left. There is also little upwards movement of the soil, this confirms what the instrumentation showed, that the initial accelerations were lower for test 2 than test 1.

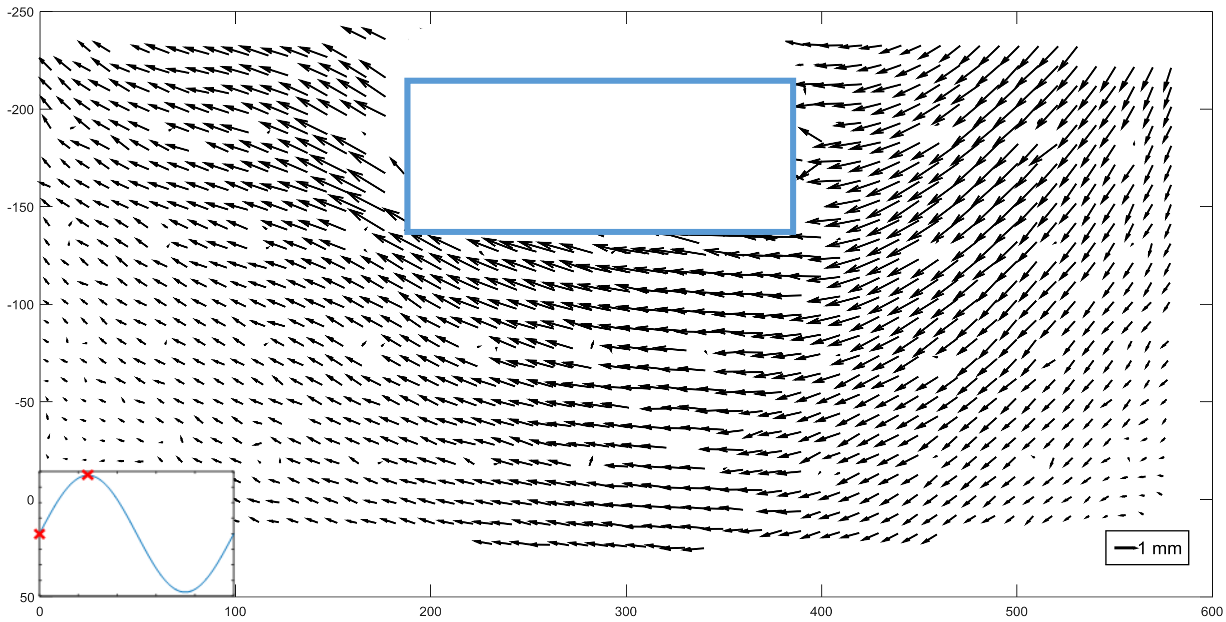

Figure 41 – First Quarter of Cycle for Test 2

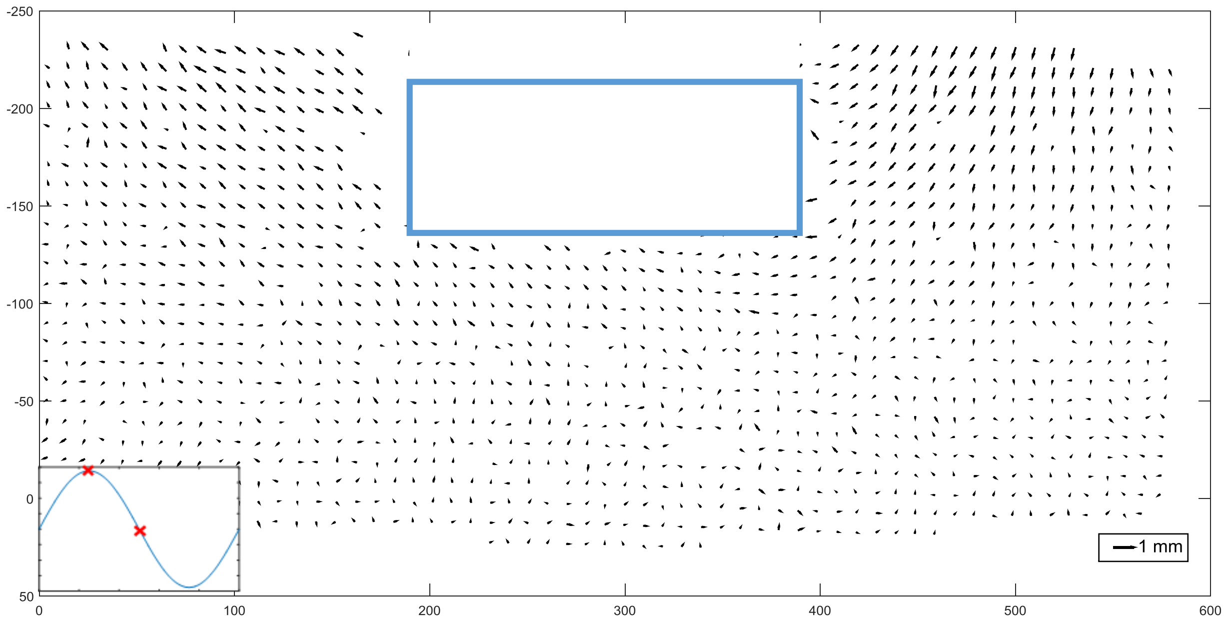

Figure 42 - Second Quarter of Cycle for Test 2

Figure 42 shows the second quarter of the first cycle, this plot shows very little soil movement after the first reversal in direction of the model. A possible explanation for this could be that before the soil liquefied the higher viscosity fluid held the soil in position relative to the model container resulting in much lower soil movements.

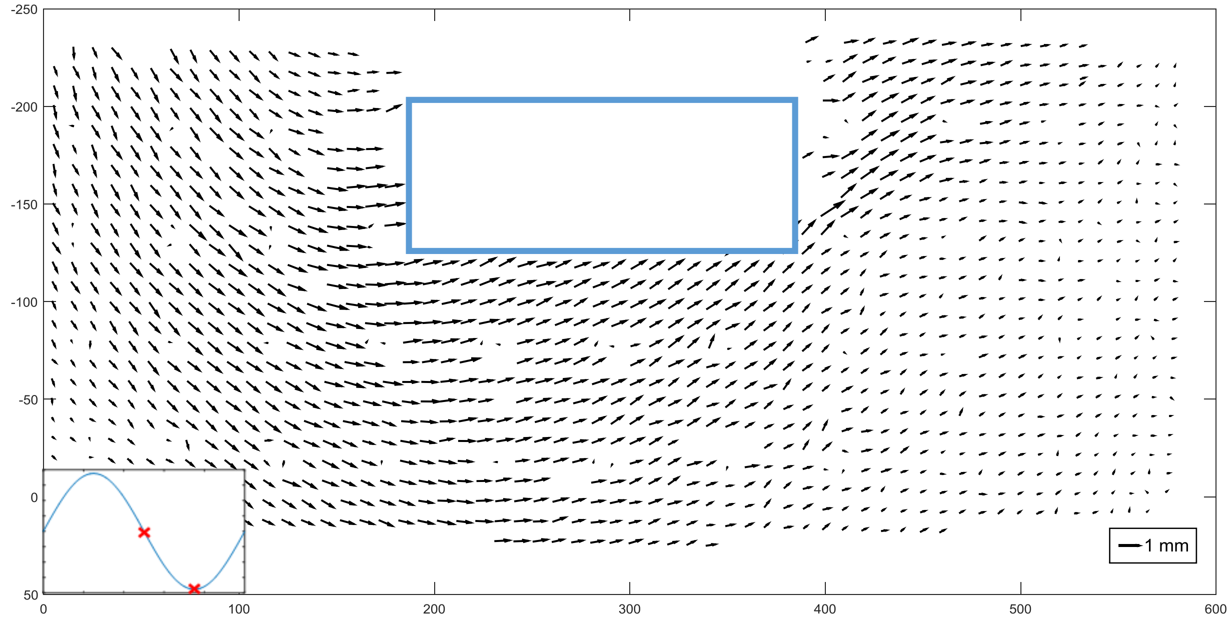

Figure 43 - Third Quarter of Cycle for Test 2

Figure 43 shows the third quarter of the first cycle, soil movement here is now in the same direction as in test 1 but still of much lower magnitude. At this stage the soil movement surrounding the tunnel is similar to that in test 1 but there are larger undisturbed areas further from the tunnel.

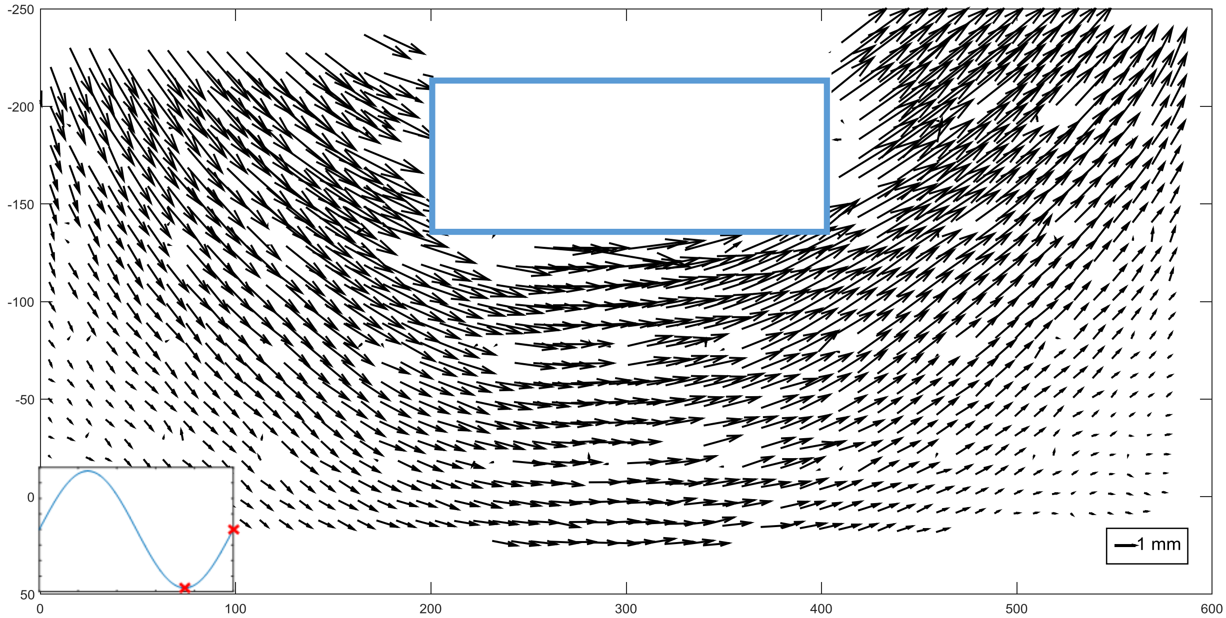

Figure 44 - Fourth Quarter Cycle for Test 2

Figure 44 shows the fourth quarter of the first cycle for test 2. At this stage the direction of all vectors are very similar to those in test 1 but they are all of lower magnitude. As was the case in figure 43 this is likely to be the result of the higher viscosity fluid increasing friction with the container walls and between soil particles thereby reducing movement relative to the container. The reduced soil displacement shown in figures 41 to 44 explains the reduced tunnel uplift seen in test 2.

6.3 Test 3 – Viscosity 30.2 Centistoke

Figure 45 shows the soil surface profile before and after test 3. The maximum settlement here was 17 mm, clearly as the tunnel suffered less uplift than in previous tests less settlement of surrounding soil would be expected to occur.

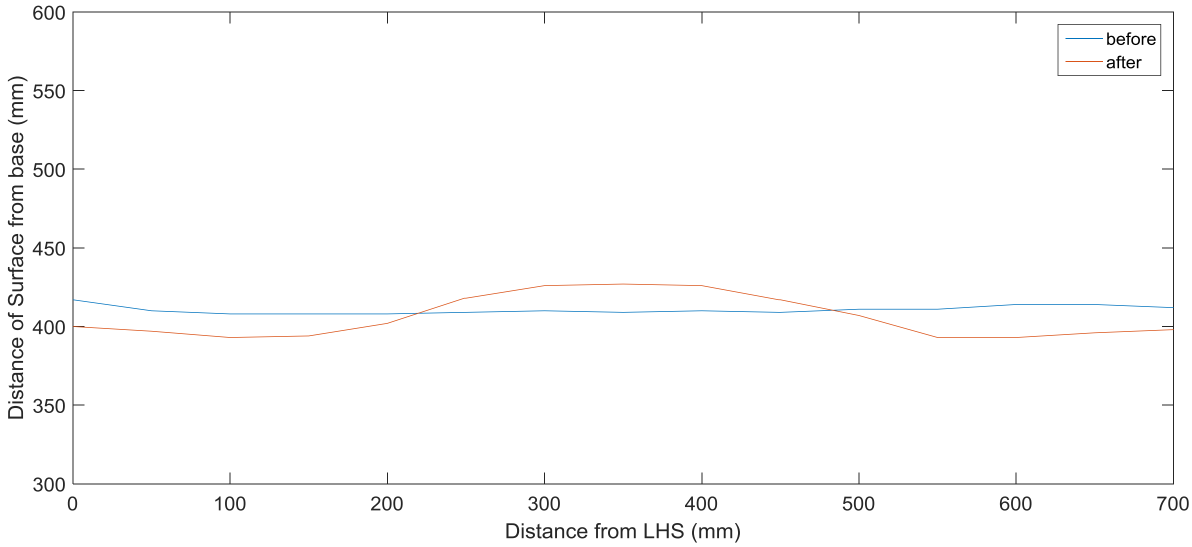

Figure 45 - Soil Surface Profile for Test 3

Figure 46 shows the cumulative soil displacement for test 3. The mechanism is similar to that seen in test 2 but with larger relatively undisturbed regions further from the tunnel.

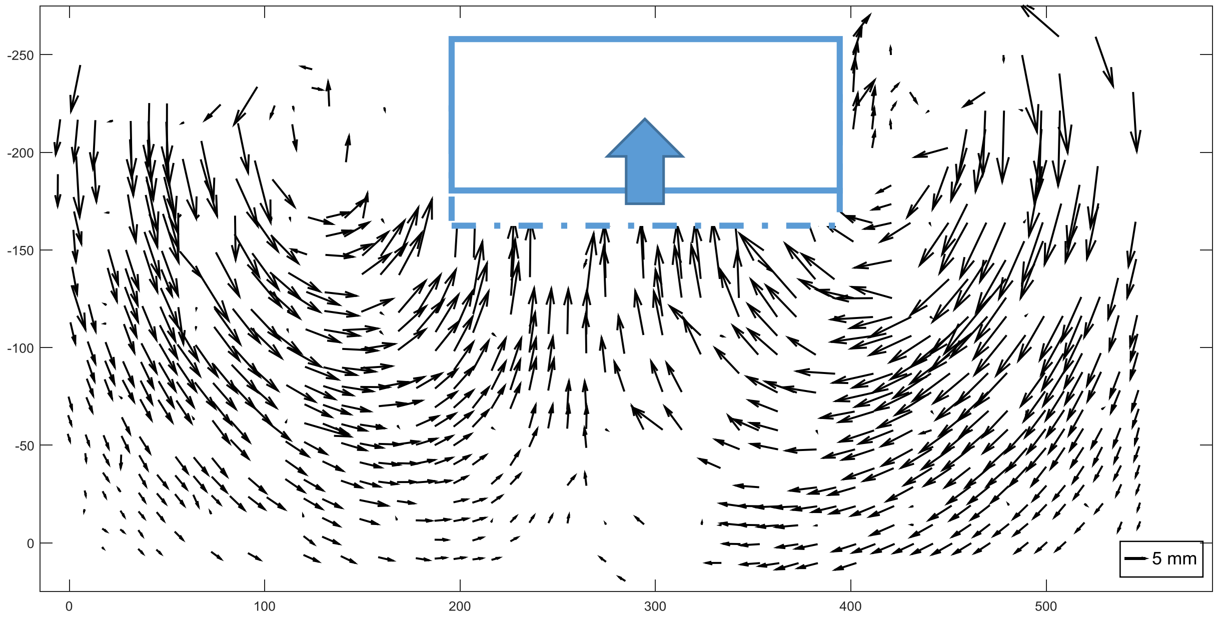

Figure 46 - Cumulative Soil Displacement for Test 3

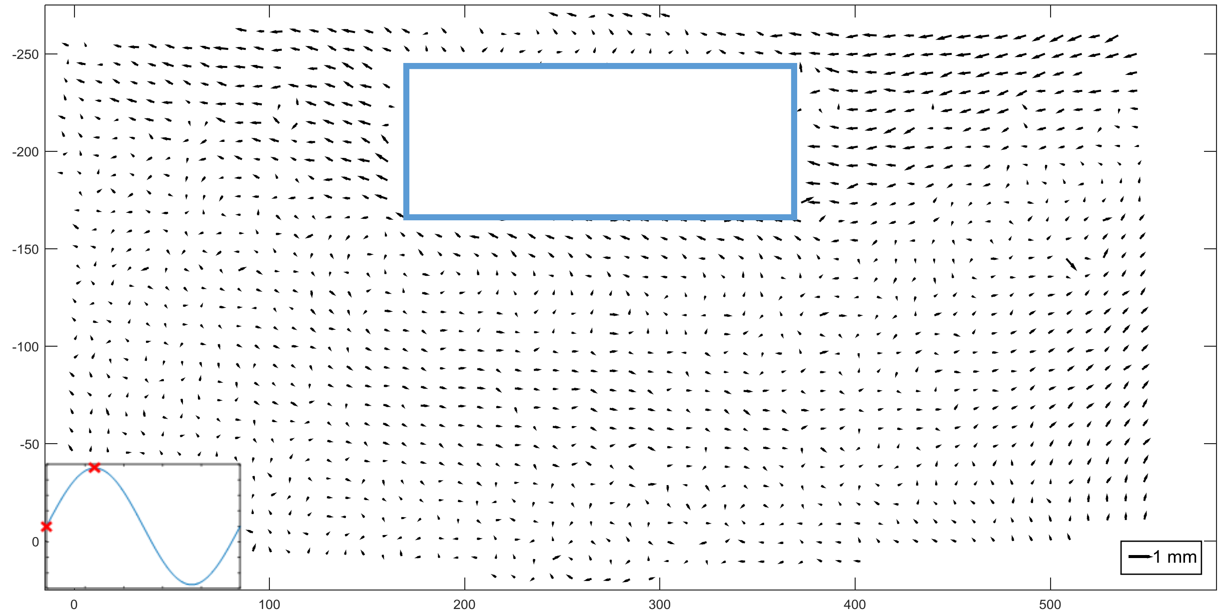

Figure 47 - First Quarter of Cycle for Test 3

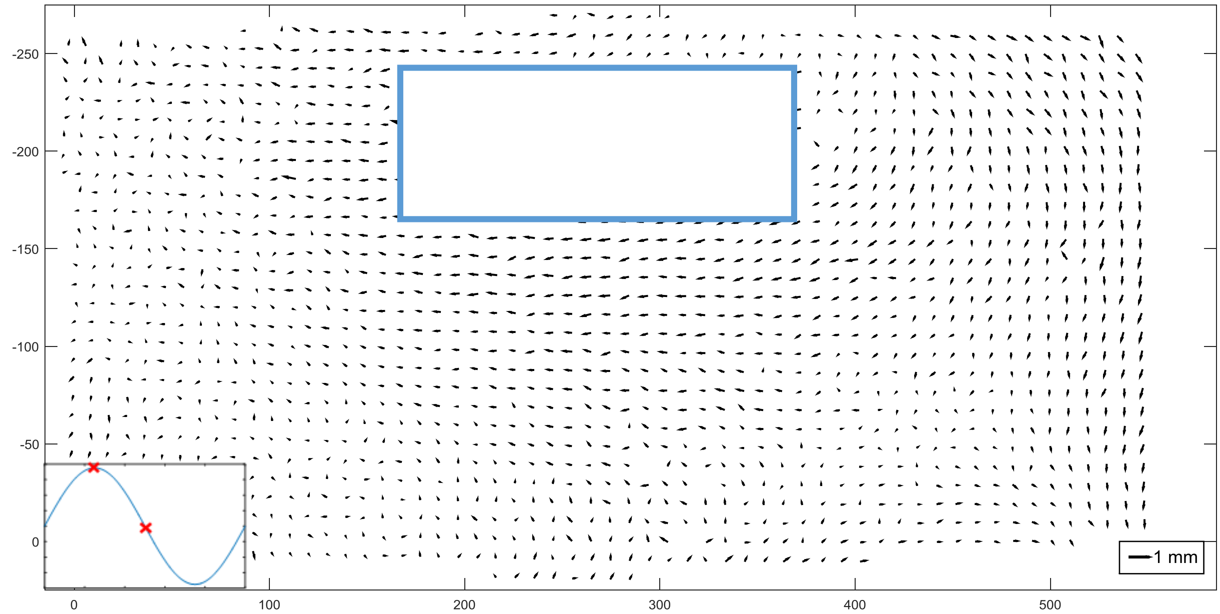

Figure 48 - Second Quarter of Cycle for Test 3

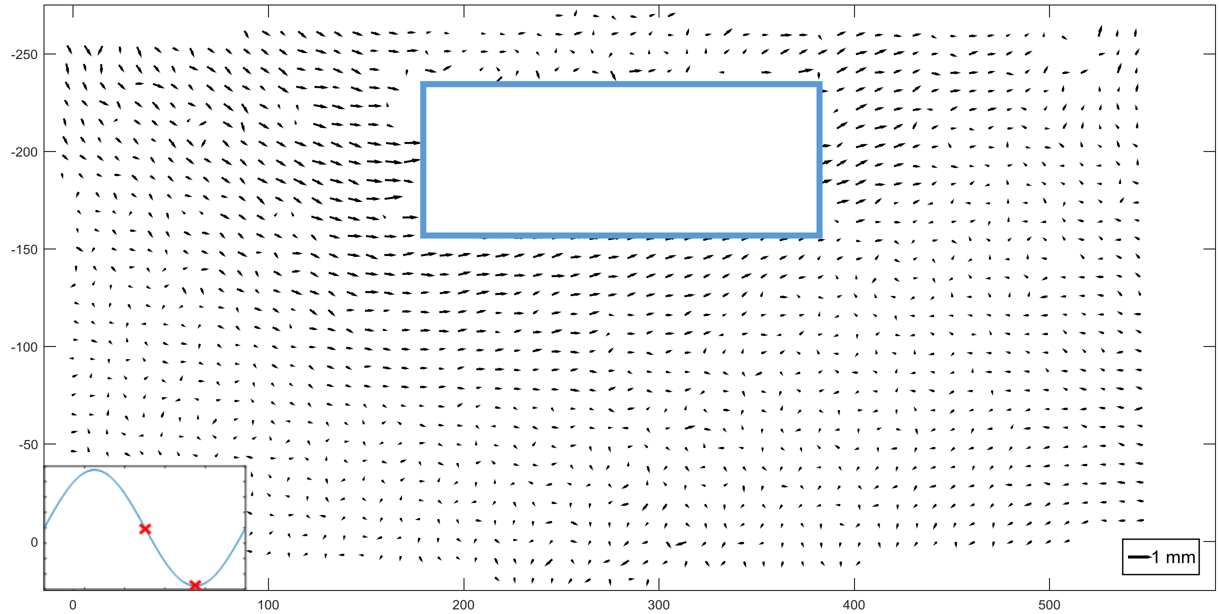

Figure 49 - Third Quarter of Cycle for Test 3

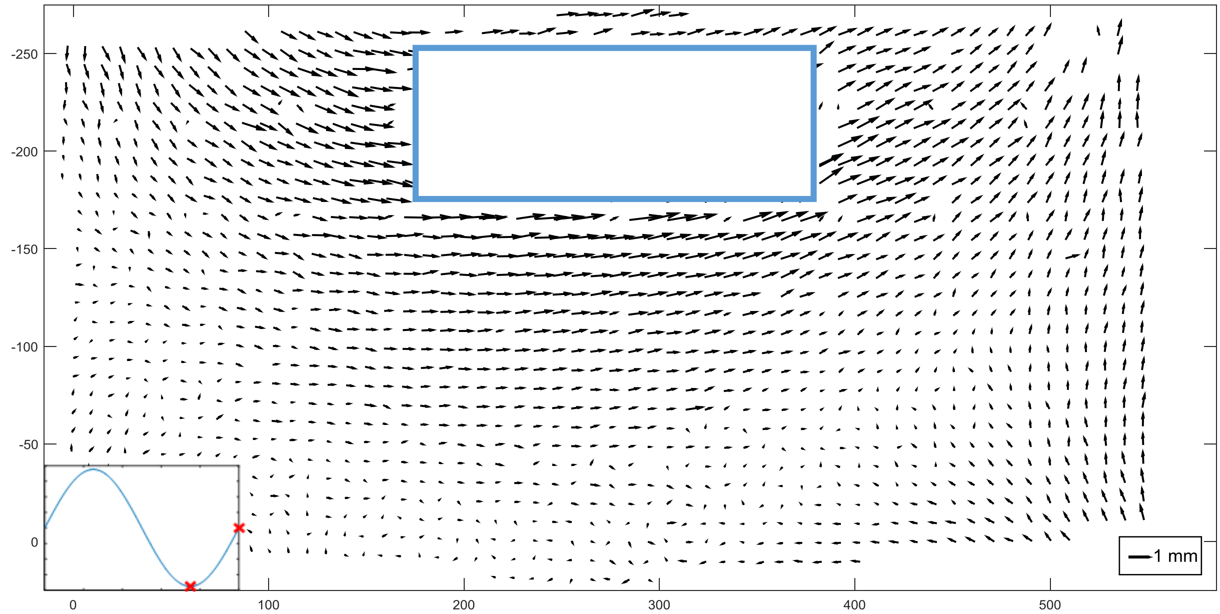

Figure 50 – Fourth Quarter of Cycle for Test 3

Figures 47 to 50 show the four quarters of the first cycle of shaking for test 3, the soil movement observed here is very similar to that seen in test 2 but with the magnitude of all vectors scaled down significantly. The result of this is that soil movement is confined to a localised region surrounding the tunnel.

6.4 Test 4 – Viscosity 3.8 Centistoke

Figure 51 shows the surface profile for test 4 before and after shaking. The maximum settlement that occurred here was 16 mm.

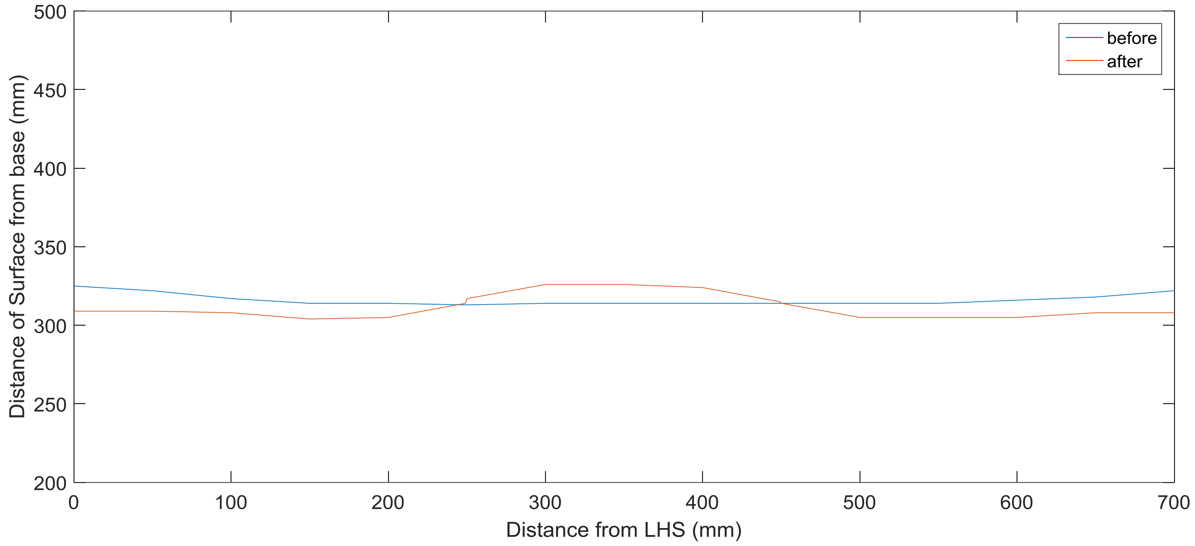

Figure 51 - Surface Profile for Test 4

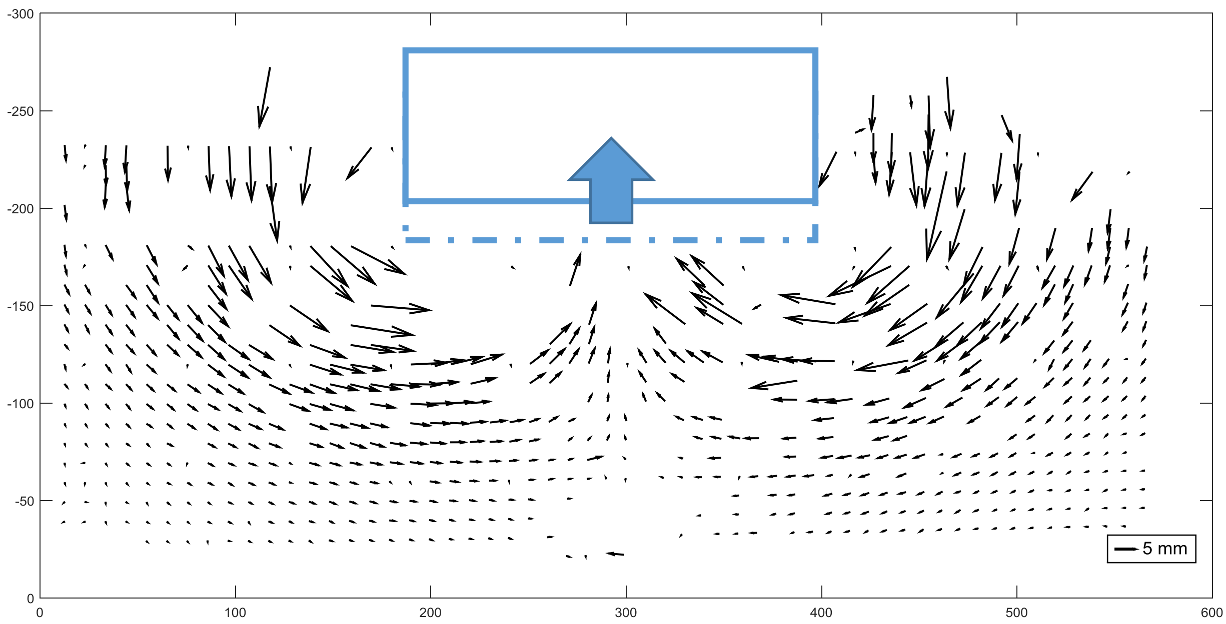

Figure 52 - Cumulative Soil Displacement for Test 4

Figure 52 shows the cumulative soil displacement for test 4, the mechanism is similar to that seen in other tests, one key difference is that the soil that was displaced by the shaking seems to be limited to a region closer to the tunnel than in previous tests.

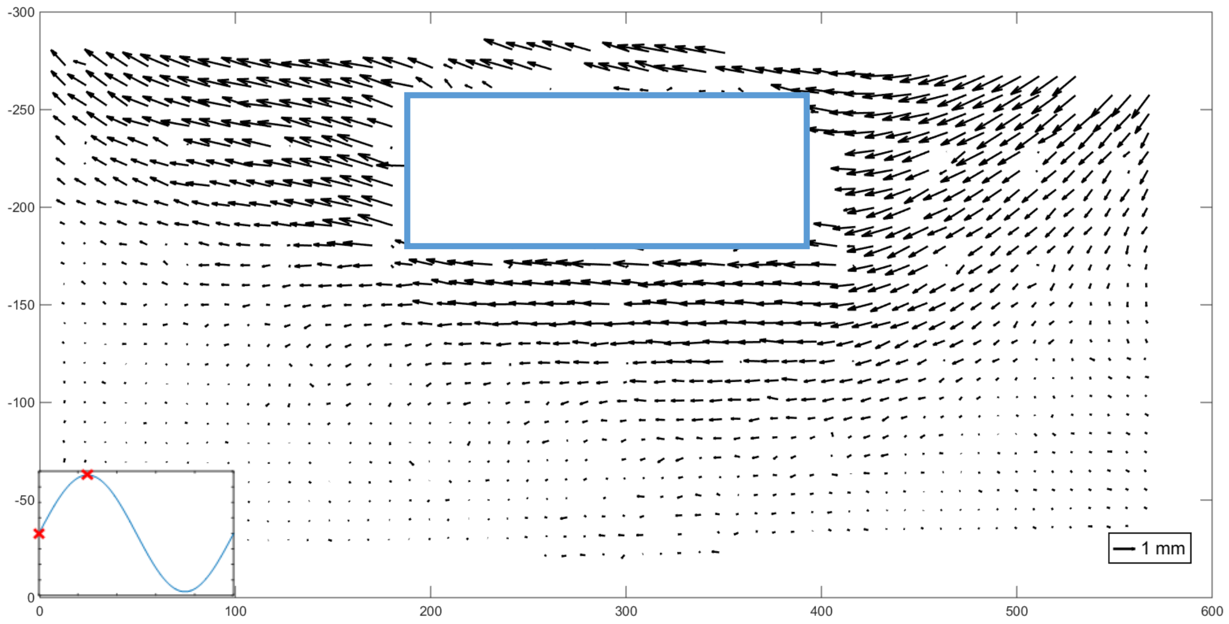

Figure 53 - First Quarter of Cycle for Test 4

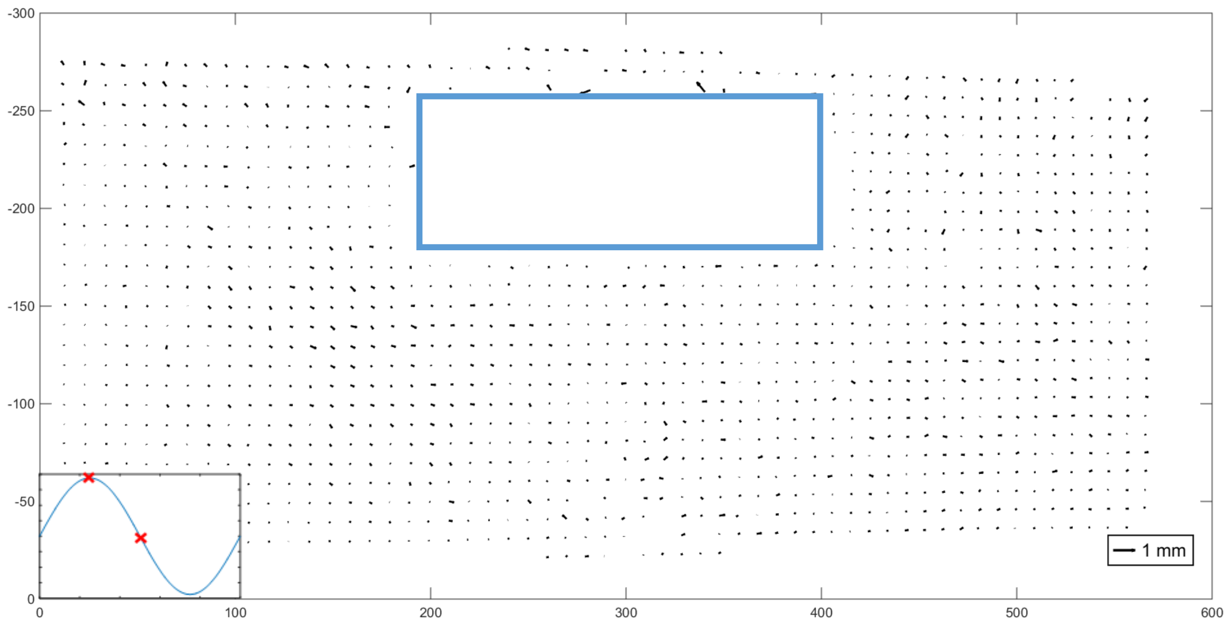

Figure 54 - Second Quarter of Cycle for Test 4

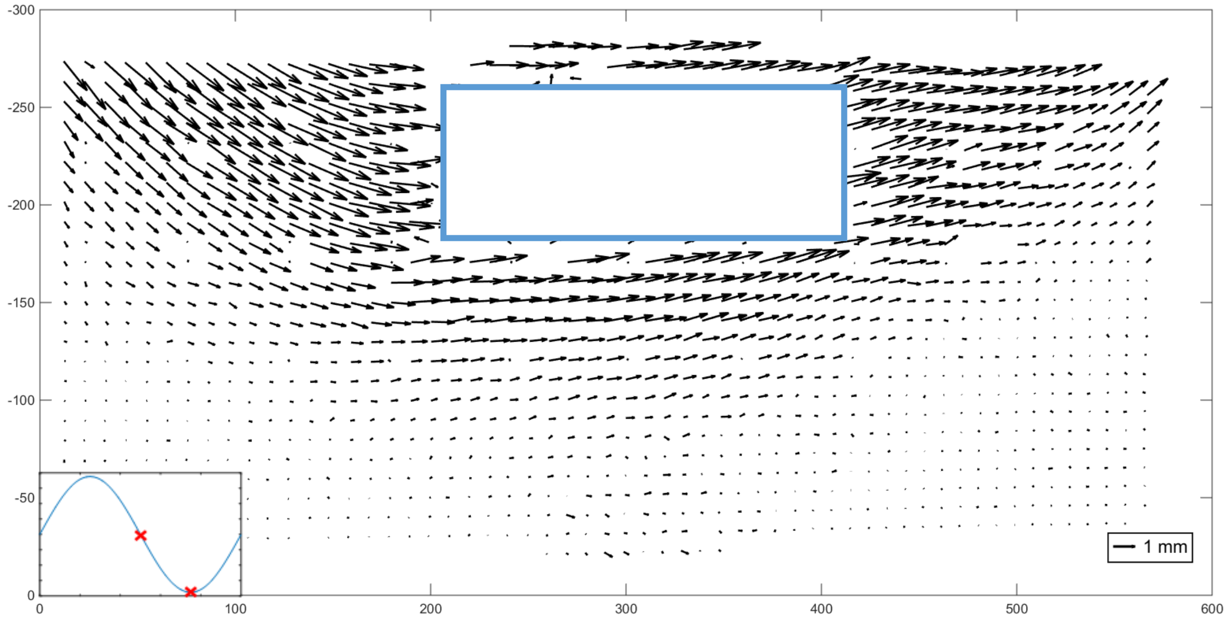

Figure 55 - Third Quarter of Cycle for Test 4

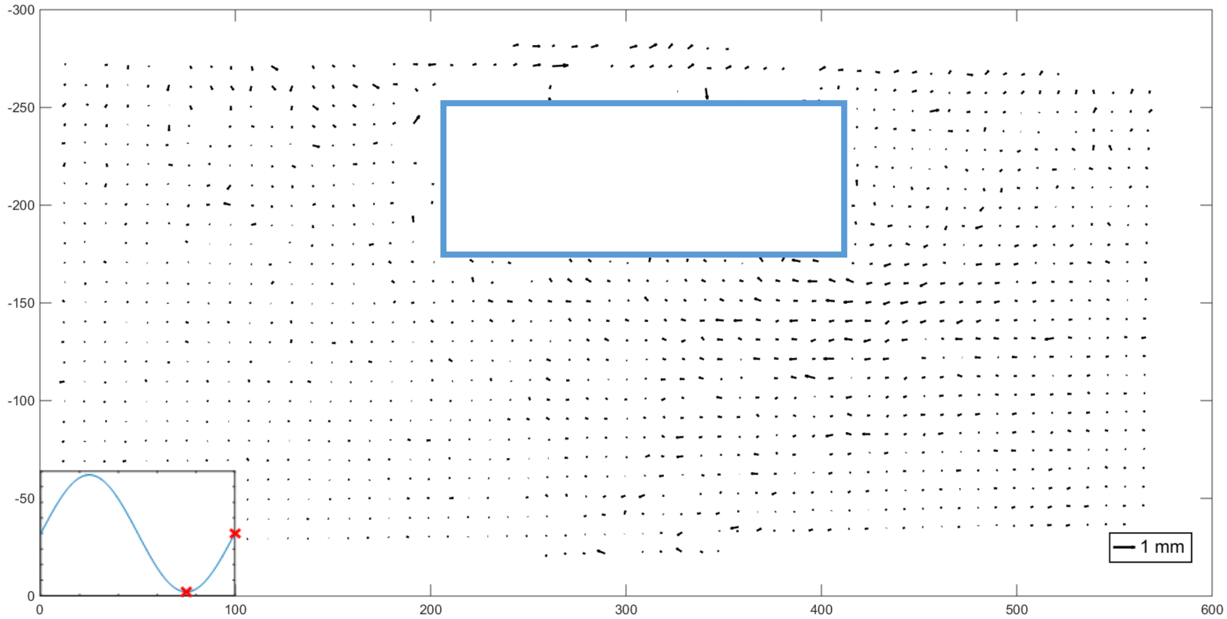

Figure 56 - Fourth Quarter of Cycle for Test 4

Figures 53-56 show separately the four quarters of the first cycle for test 4, these figures go some way towards explaining why the tunnel floated less in test 4 than in any other test. Clearly in the quarters where the tunnel is returning to the central position there is almost no soil movement. Soil movement in other quarters is more similar to that seen in other tests except that vectors are of larger magnitude than those seen in test 3 and smaller than those seen in tests 1 and 2, another difference is that soil movement seems to be confined to a smaller region surrounding the tunnel than in other tests. This reduced soil movement would clearly lead to reduced tunnel uplift.

7 CONCLUSIONS

This report has covered observations made during this investigation and attempted to provide some explanation of the findings. This section contains the conclusions that can be drawn from the work carried out:

- Pore fluid viscosity clearly has an impact on tunnel uplift. Soil permeability will have a similar impact, as increasing fluid viscosity has the same effect on fluid movement through the soil as decreasing permeability
- The relationship between pore fluid viscosity and tunnel uplift is in no way linear. Generally increasing viscosity decreases uplift however, results obtained here indicate that there is a region between 1 and 10 CSt where uplift will be lower than at higher viscosities. Excluding the result in test 4, tunnel uplift seems to decrease exponentially with viscosity - it is likely that the result of test 4 was an anomaly and a result of some experimental error. Quite possibly the sand was denser than in previous tests due to the inconsistent nature of manual sand pouring
- Rate of tunnel uplift also declines with increasing viscosity - vertical acceleration experienced by the tunnel is linked to the fluid viscosity. In higher viscosity fluids, the tunnel experiences more consistent acceleration over the full period of shaking. This may be because at low viscosity (1 CSt) the tunnel floats rapidly early in the test reaching an equilibrium so that no further acceleration occurs
- Pore fluid viscosity has an impact on the rate at which pore pressures can be dissipated in the soil and the suction force acting on the base of the tunnel. The interaction between these two factors plays a significant role in determining tunnel uplift
- Tunnel uplift is closely related to the magnitude of soil movements surrounding the tunnel and the extent of the area of soil movement. Although, from the results obtained here, it cannot be ascertained whether the reduced magnitude of soil movement is caused by the reduced tunnel movement or vice versa

- Shaking leads to settlement of soil surrounding the tunnel with the amount of settlement linked to the uplift of the tunnel. The settlement is the combined result of densification of the sand and movement of the sand to fill the void left behind the tunnel as it moves upwards
- The GoPro recording at 60 fps provides images that can be used to look at soil displacements over short periods however, over larger ranges of images the results produced using the GoPro are of insufficient quality to carry out detailed analysis with lots of data being lost to wild vectors

8 FUTURE WORK

As with many investigations in the field of engineering this project raises as many questions as answers. Below are suggestions for expansion of the work carried out here that may possibly answer some of the uncertainties uncovered in this work and allow application of results in solving real life problems:

- Investigation into the impact of pore fluid viscosity on tunnel uplift between 1 and 10 CSt to verify the result of test 4 in this investigation
- Investigation using a fluid with viscosity lower than 1 CSt to provide interesting data on the effect of higher permeability soils on tunnel floatation, and show whether at high enough permeabilities no floatation would occur as pore pressures are drained away too rapidly for soil liquefaction to occur
- The tests carried out here could be repeated using a longer shaking duration to see if the maximum tunnel uplift was limited purely as an equilibrium had been reached or because at the lower rate of uplift in higher viscosity fluids the total uplift was limited by the duration of the test
- Carrying out tests on a tunnel model that has been adapted with measures to prevent floatation would be interesting and possibly provide a real life application of the results
- Repeating the tests carried out here in the centrifuge so that stresses are properly scaled would be useful to check the validity of the data and to provide information more useful in a life size situation
- In order to truly compare the GoPro and high speed camera in their effectiveness for use in PIV, both cameras could be used to record the same tests and then the resulting PIV data from each compared

9 REFERENCES

[1] United States Geological Survey, “Earthquake Facts,” 7 April 2016. [Online]. Available: http://earthquake.usgs.gov/learn/facts.php. [Accessed 4 May 2016].

[2] United States Geological Survey, “Magnitude 9.1 - Off the West Coast of Northern Sumatra,” 28 January 2015. [Online]. Available: http://earthquake.usgs.gov/earthquakes/eqinthenews/2004/us2004slav/#details. [Accessed 4 May 2016].

[3] United States Geological Survey, “Magnitude 7.6 - Pakistan,” 7 October 2010. [Online]. Available: http://earthquake.usgs.gov/earthquakes/eqinthenews/2005/usdyae/#details. [Accessed 4 May 2016].

[4] United States Geological Survey, “Magnitude 7.9 - Eastern Sichuan, China,” 28 January 2015. [Online]. Available: http://earthquake.usgs.gov/earthquakes/eqinthenews/2008/us2008ryan/#details. [Accessed 4 May 2016].

[5] United States Geological Survey, “Magnitude 7.0 - Haiti Region,” 28 January 2015. [Online]. Available: http://earthquake.usgs.gov/earthquakes/eqinthenews/2010/us2010rja6/#details. [Accessed 4 May 2016].

[6] United States Geological Survey, “Magnitude 9.0 - Near the East Coast of Honshu, Japan,” 23 March 2015. [Online]. Available: http://earthquake.usgs.gov/earthquakes/eqinthenews/2011/usc0001xgp/#details. [Accessed 4 May 2016].

[7] C. Clifton, “Christchurch Feb 22nd Earthquake: A Personal Report by Charles Clifton - March 2011,” March 2011. [Online]. Available: http://www.hera.org.nz/Story?Action=View&Story_id=1398. [Accessed 4 May 2016].

[8] Government of Nepal, “Incident Report of Earthquake 2015,” 2015. [Online]. Available: https://web.archive.org/web/20150629024928/http://drrportal.gov.np/incidentreport. [Accessed 4 May 2016].

[9] Wikimedia Commons, “Liquefaction of Niigata,” 1964. [Online]. Available: https://commons.wikimedia.org/wiki/File:Liquefaction_at_Niigata.JPG. [Accessed 4 May 2016].

[10] Wikimedia Commons, “Chuetsu Earthquake Liquefaction,” 2004. [Online]. Available: https://commons.wikimedia.org/wiki/File:Chuetsu_earthquake-earthquake_liquefaction1.jpg. [Accessed 4 May 2016].

[11] Schwede66, “River Road,” 25 February 2011. [Online]. Available: https://commons.wikimedia.org/wiki/File:25_Feb_2011_River_Road.jpg. [Accessed 4 May 2016].

[12] R Dobry, “Some Basic Aspects of Soil Liquefaction during Earthquakes,” *Earthquake Hazards and the Design of Constructed Facilities in the Eastern United States,* vol. 558, pp. 172-182, 1989.

[13] Seed et al, “Recent Advances in Soil Liquefaction Engineering: A Unified and Consistent Framework,” Earthquake Engineering Research Centre, College of Engineering, University of California, Berkeley, 2003.

[14] SSC Madabhushi & SPG Madabhushi, “Finite element analysis of floatation of rectangular tunnels,” CUED, Cambridge, 2014.

[15] M Stringer & SPG Madabhushi, “MODELLING OF LIQUEFACTION AROUND TUNNELS,” in *4th International Conference on Earthquake Geotechnical Engineering*, Thessaloniki, 2007.

[16] M. Jenkins, “Characterisation of Floatation of Rectangular Tunnels Following Earthquake Induced Liquefaction,” CUED, Cambridge, 2015.

[17] E. Room, “Visualisation of floatation of tunnels following earthquake induced liquefaction,” CUED, Cambridge, 2014.

[18] O Adamidis & SPG Madabhushi, “On preparation of viscous pore fluids,” CUED, Cambridge, 2014.

[19] D White & W Take, “GeoPIV: Particle Image Velocimetry (PIV) software for use in geotechnical testing,” CUED, Cambridge, 2002.

[20] D White, W Take & M Bolton, “Soil deformation measurement using particle image velocimetry (PIV) and photogrammetry,” *Ge´otechnique,* vol. 53, no. 7, p. 619–631, 2003.

[21] H Mitrani, “Liquefaction Remediation Techniques for Existing Buildings,” CUED, Cambridge, 2006.

10 Appendices

10.1 Appendix 1 – Buoyancy Calculation

The calculation for net force on the tunnel used here is the same as that used by Jenkins (2015) in his investigation into floatation of tunnels.

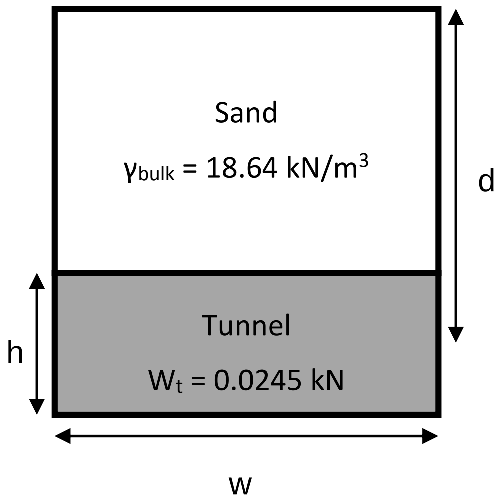

Dimensions

w = 200 mm

h = 80 mm

L = 300 mm

d = 70 mm

Sand Properties

Specific Gravity, G_s = 2.65

Voids Ratio, e ≈ 0.828

e_{max} = 1.01 [21]

e_{min} = 0.555 [21]

Relative Density, I_D ≈ 40%

Bulk Unit Weight, γ_{bulk} ≈ 18.64 kN/m^3

Figure 57 - Model Properties for Buoyancy Calculation

$$F_{up} = whL\gamma_w = 0.200 \times 0.080 \times 0.300 \times 9.81 = 0.047\ kN$$

$$F_{down} = W_t + \left(d - \frac{h}{2}\right) wL[\gamma_{bulk} - \gamma_w]$$

$$= 0.0245 + \left(0.070 - \frac{0.080}{2}\right) \times 0.200 \times 0.300 \times [18.64 - 9.81]$$

$$= 0.040\ kN$$

$$F_{net} = F_{up} - F_{down} = 0.047 - 0.040 = \boxed{0.007\ kN}$$

Equation 5 - Buoyancy Force Calculation

10.2 Appendix 2 – Risk Assessment Review

Before the start of this project a risk assessment was completed in order to identify and reduce known risks involved with the work. During the project further risks were identified and appropriate measures taken to address them. These additional risks are detailed here in the hope that they will be useful for anyone looking to develop on the work carried out in this investigation:

- **Inhalation of sand particles during sand pouring** – This could lead to potential short term breathing difficulties and discomfort, or over long term exposure, permanent damage to the lungs. This risk was minimised through the use of dust extraction units where available and individual full face masks where use of the dust extraction units was not feasible
- **Manual handling of large sand pouring hopper** – Potential for injury to occur during lifting either muscular or crushing. This risk was overcome by using two people to lift the hopper and also wearing steel toe cap boots to protect feet, where possible the hopper was moved using an overhead crane
- **Potential health hazard from bacteria propagating in Methyl Cellulose solution** – Although initially methyl cellulose is free of bacteria it does provide an ideal environment in which bacteria can thrive if for example an insect was to become trapped and die in the fluid, this was avoided by always keeping the solution covered
- **Risk of burns due to heat generated by lighting** – The halogen lights used for PIV generate significant amounts of heat, the risk of burns was minimised by keeping the lights switched off except for the duration of the test and allowing sufficient time for them to cool before handling them following a test
- **Inhalation of volatile solvents from blue dye** – The blue dye used to colour the sand contains volatile solvents which may cause dizziness if inhaled, the risk of this was minimised by wearing a face mask during use of the dye and also ensuring a plentiful supply of fresh air during the dyeing process